Applied Physics Reviews

Perovskite photonic crystal photoelectric devices

Cite as: Appl. Phys. Rev. **9**, 041319 (2022); https://doi.org/10.1063/5.0106118
Submitted: 27 June 2022 • Accepted: 30 November 2022 • Published Online: 16 December 2022

Yanan Ji, Wen Xu, Ilia L. Rasskazov, et al.

AIP Publishing

Applied Physics Reviews REVIEW scitation.org/journal/are

Perovskite photonic crystal photoelectric devices

Cite as: Appl. Phys. Rev. **9**, 041319 (2022); doi: 10.1063/5.0106118
Submitted: 27 June 2022 · Accepted: 30 November 2022 ·
Published Online: 16 December 2022

View Online Export Citation CrossMark

Yanan Ji,[1] Wen Xu,[1,2,a)] Ilia L. Rasskazov,[3] Haichun Liu,[4] Junhua Hu,[5] Mao Liu,[6] Donglei Zhou,[2] Xue Bai,[2] Hans Ågren,[7] and Hongwei Song[2,a)]

AFFILIATIONS

[1]Key Laboratory of New Energy and Rare Earth Resource Utilization of State Ethnic Affairs Commission, Key Laboratory of Photosensitive Materials & Devices of Liaoning Province, School of Physics and Materials Engineering, Dalian Minzu University, 18 Liaohe West Road, Dalian 11660, China
[2]State Key Laboratory of Integrated Optoelectronics, College of Electronic Science and Engineering, Jilin University, Changchun 130012, China
[3]Institute of Optics, University of Rochester, 275 Hutchison Road, Rochester, New York 14627, USA
[4]Department of Applied Physics, KTH Royal Institute of Technology, SE-106 91 Stockholm, Sweden
[5]State Centre for International Cooperation on Designer Low-Carbon and Environmental Materials, School of Materials Science and Engineering, Zhengzhou University, Zhengzhou 450001, China
[6]School of Metallurgy, Northeastern University, Shenyang 110819, China
[7]Department of Physics and Astronomy, Uppsala University, Box 516, SE-751 20 Uppsala, Sweden

[a)]**Authors to whom correspondence should be addressed:** xuwen@dlnu.edu.cn and songhw@jlu.edu.cn

ABSTRACT

Metal halide perovskite materials have been extensively explored in modern photonic devices. Photonic crystals (PCs) are periodic structures with specific optical properties, such as photonic stop bands and "slow photon" effects, which can tailor the propagation and distribution of photons in photoelectric devices. PCs have in recent years been widely explored to significantly improve the performance of perovskite luminescent materials and/or photoelectric devices. Therefore, a full understanding of the key role of PCs and a further learning of the correct use of PCs in perovskite photonic/photoelectric devices are essential for realizing the inherent potential of the superior performance of such devices. By means of this first review, we aim at offering a comprehensive framework description for PCs suitable for high-performance perovskite photoelectric devices. We start with a brief introduction to the basic aspects of PCs. Then, we summarize the influences of PCs on emission/absorption for perovskite luminescent materials. Subsequently, we systematically discuss concepts like light extraction, light trapping, slow-light effects, and structural effects of PCs for perovskite devices, with a particular emphasis on their theoretical descriptions. We argue that the marriage of perovskite materials with PCs can open up a novel frontier in photoelectric devices that potentially can spawn many exciting new fields.

TABLE OF CONTENTS

I. INTRODUCTION

Over the past decade, metal halide perovskite materials, organic–inorganic as well as all-inorganic, have attracted enormous attention due to their high absorption coefficients, extraordinary charge carrier transport properties, long charge-carrier diffusion length, tunable bandgap with efficient emission, and economic cost for commercial use.[1–8] In general, hybrid halide perovskites process the typical crystal structure with the chemical formula of ABX_3, where A represents a monovalent organic or inorganic cation [MA^+: $CH_3NH_3^+$, FA^+: $HC(NH_2)_2^+$, or Cs^+], B presents a metal cation (Pb^{2+}, Sn^{2+}, or Eu^{2+}), and X is a halide anion (typically Cl^-, Br^-, and I^-, or mixtures thereof).[9,10] They exhibit excellent performance for various optoelectronic applications, for example, solar cells (SCs),[11–20] light-emitting diodes (LEDs),[6,8,21–28] photodetectors (PDs),[29–34] phototransistors,[35] and lasers.[36–42]

The first demonstration of metal halide perovskite materials concerned organic–inorganic (MA^+, FA^+) metal halide perovskites by Weber in the 1970s.[43] In 2009, Kojima *et al.*[44] first employed $MAPbBr_3$ and $MAPbI_3$ as the photosensitizer to develop perovskite solar cells (PSCs) and obtained initially a power conversion efficiency (PCE) of around 3.8%. After that, all-inorganic halide perovskites with excellent stability, optical, and electrical properties, especially for $CsPbX_3$ ($X = Cl^-$, Br^-, I^-, or their mixtures), have been widely explored.[11,25,40,45–48] They were synthesized in 1958 by Møller,[49] and a significant recent progress was achieved by Protesescu *et al.*[25] in 2015 who synthesized $CsPbX_3$ nanocrystals (NCs) with tunable bandgap covering the entire visible spectral region spanning from 410 to 700 nm, obtaining a photoluminescence quantum yield (PLQY) over 90% for green $CsPbBr_3$ NCs. After over 10 years of rapid development, metal halide perovskite materials have been developing over various dimensions, typically including zero-dimensional [e.g., quantum dots (QDs), NCs, and nanoparticles (NPs)],[1,8,21,40,46,48,50,51] one-dimensional (1D),[52–55] two-dimensional (2D),[56,57] and three-dimensional (3D),[17] and their hybrids (e.g., 2D-3D hybrids).[58] Great improvements have been obtained for the PCE of the PSCs, reaching an amazing 25.2%.[59] The near-unity PLQY of metal halide perovskite materials can be achieved over the wavelengths covering the wavelength from 400 to 700 nm.[50,51,60] A series of blue, green, red, and near-infrared LEDs has been realized with the external quantum efficiency (EQE) exceeding 22%.[23] The perovskite PDs with high responsivity, detectivity, and EQE have also been achieved spanning from high-energy x-ray, deep-ultraviolet (UV) to near-infrared light.[61–65] The above-reviewed applications based on perovskite materials all relate to emission and absorption of light, photoelectric conversion, and electro-optic conversion. A number of approaches have been carried out to boost the performance of perovskite photoelectric devices, and extreme achievements have been obtained. Generally, surface passivation, ion doping, device structure optimization, and energy bandgap engineering have been implemented to enhance the PLQY and overall performance of perovskite devices through reducing the non-radiative rate of the perovskite materials or enhancing the carrier injection/extraction efficiency in the devices. Differently, light management based on photonic crystals serves also as a promising method to largely improve the performance of perovskite photonic and photoelectric devices.[66–71]

Photonic crystals (PCs), classified into 1D, 2D, and 3D PCs,[71] composed of periodically repeated units with different dielectric constants (or refractive indices) of materials, were first explored by John and Yablonovitch in 1987.[72,73] The PCs can generate unique photonic bandgaps (PBGs) when their periodicities are comparable to the wavelength of photons, in which photon propagation through the PCs can be precisely controlled.[74,75] Because of this capability, PCs are generally used to boost the performance of perovskite devices in several ways.[76,77]

First, spontaneous light emission of perovskite materials represents a photon emission process where an electron in an excited state returns to a lower-energy state or ground state through releasing a photon. The photoluminescence (PL) produced by spontaneous emission, competing with non-radiative decay, plays a crucial role for the highly efficient luminescence and internal PLQY in LEDs of perovskites. PCs can spontaneously boost the light emission via the Purcell effect to improve the PLQY of perovskites.[67] PCs can also inhibit spontaneous light emission and redistribute the light energy to increase the extraction efficiency of LEDs.[78] In addition, recent advances in light–matter interaction in perovskite, such as phase change with polarization tuning,[79] chirality,[80] and optical Rashba effect,[79,81] are also important for the development of perovskite photonics.

Second, light trapping and slow-photon effects in PCs can enhance the photon incoupling and photon recycling in perovskites, thereby significantly boosting light utilization, contributing to high performance of the PSCs and PDs. In addition, the porous structure of PCs implies a high surface-to-volume ratio and scattering efficiency and affords a highly crystalline perovskite film as well.

Herein, we comprehensively review the recent progresses in the field of PCs applied for high-performance perovskite photoelectric devices. We start with a brief introduction to the fundamental aspects of PCs. Next, we discuss the effects of PC structures on spontaneous emission for luminescent perovskite materials. Then, we systematically discuss the light extraction, light trapping, the slow-light effect, and structural effects of PCs for lasing, LEDs, PSCs, and PDs as leading examples, with a particular emphasis on their theoretical descriptions and applications. The progress in the research for perovskite photoelectric crystals is summarized in Schematic 1. Finally, we highlight possible paths for the future development of PC-based perovskite photoelectric devices.

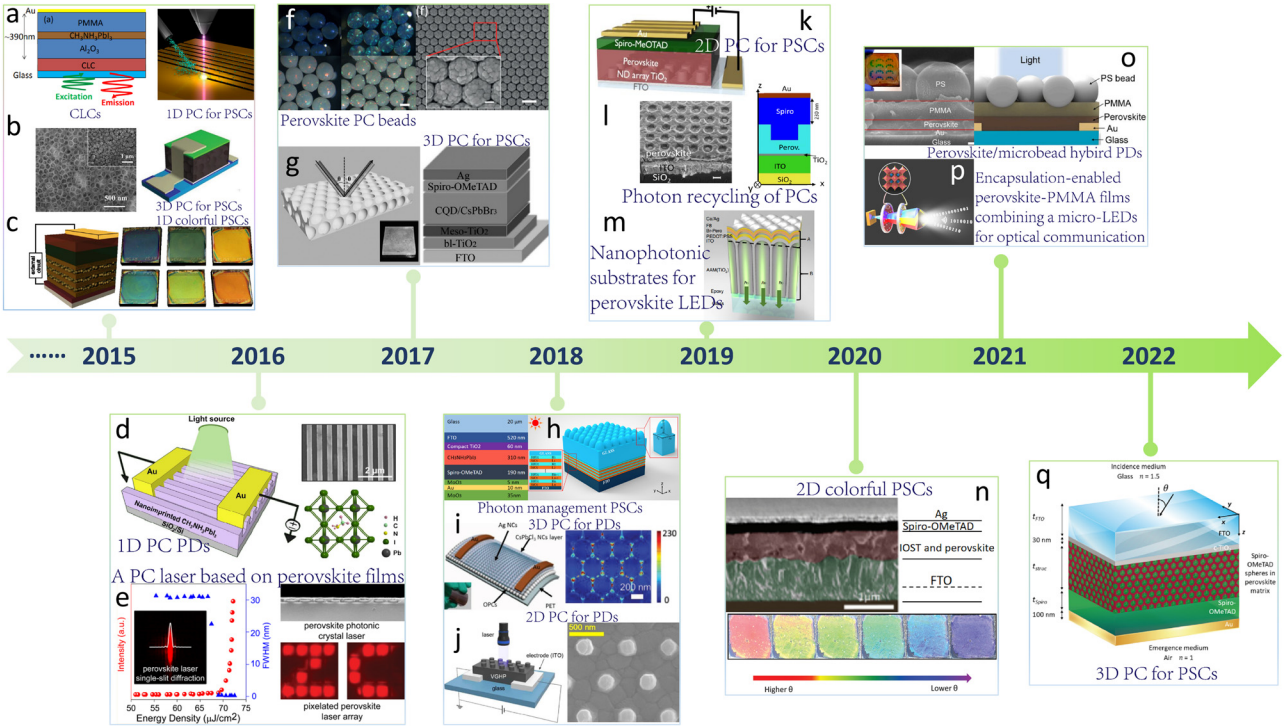

SCHEME 1. A timeline of the progress in the research for perovskite photoelectric crystals. (a) In 2015, Stranks *et al.* were the first to demonstrate enhanced amplified spontaneous emission in perovskites using a flexible cholesteric liquid crystal reflector.[82] Reproduced with permission from Stranks *et al.*, Nano Lett. **15**, 4935–4941 (2015). Copyright 2015 American Chemical Society. (b) Ooi *et al.* using a chemically gas-assisted focused-ion beam for subwavelength grating PSCs.[83] Reproduced with permission from Alias *et al.*, J. Phys. Chem. Lett. **7**, 137–142 (2015). Copyright 2015 American Chemical Society. (c) Chen *et al.* using opal-like TiO_2 as ETL to obtain hybrid PSCs.[84] Reproduced with permission from Chen *et al.*, Adv. Sci. **2**, 1500105 (2015). Copyright 2015 Authors, licensed under a Creative Commons Attribution (CC BY) license. (d) Snaith *et al.* integrated a porous 1D PC scaffold into a PSC, which exhibited an efficiency of 4%–9% with tunable color covering the entire visible spectrum.[85] Reproduced with permission from Zhang *et al.*, Nano Lett. **15**, 1698–1702 (2015). Copyright 2015 American Chemical Society. (e) In 2016, Walter Hu *et al.* were the first to use nanoimprint lithography to obtain nanoscale-patterned perovskite PDs.[86] Reproduced with permission from Wang *et al.*, ACS Nano **10**, 10921–10928 (2016). Copyright 2016 American Chemical Society. (f) Chen *et al.* developed a perovskite laser embedded within a 2D PC resonator through electron beam deposition.[87] Reproduced with permission from Chen *et al.*, ACS Nano **10**, 3959–3967 (2016). Copyright 2016 American Chemical Society. (g) In 2017, Chen *et al.* proposed a preparation method of waterproof organometal halide perovskite photonic crystal beads.[88] Reproduced with permission from Chen *et al.*, Angew. Chem., Int. Ed. **56**, 6648–6652 (2017). Copyright 2017 Wiley. (h) Longwei Yin *et al.* fabricated carbon-quantum-dot-sensitized inorganic $CsPbBr_3$ IO PSCs and utilized the slow-photon effect to enhance the photoelectric conversion efficiency of PSCs.[89] Reproduced with permission from Zhou *et al.*, Adv. Mater. **29**, 1703682 (2017). Copyright 2015 Authors, licensed under a Creative Commons Attribution (CC BY) license. (i) In 2018, Yimin Xuan *et al.* employed photon management structure to suppressing the negative effect of UV light on PSCs.[90] Reproduced with permission from L. Zheng and Y. Xuan, Solar Energy **173**, 1216–1224 (2018). Copyright 2018 Authors, licensed under a Creative Commons Attribution (CC BY) license. (j) Our group using plasmonic photonic crystals structures realized a two-order fluorescence enhancement of blue perovskite nanocrystals, and obtained a flexible UV PD.[77] Reproduced with permission from Li, *et al.*, Adv. Mater. **28**, 1804429 (2018). Copyright 2018 Authors, licensed under a Creative Commons Attribution (CC BY) license. (k) Chun *et al.* demonstrated a vertically grown halide perovskite nanopillar PD through a nanoimprinting crystallization technique.[91] Reproduced with permission from Chun *et al.*, ACS Nano **12**, 8564–8571 (2018). Copyright 2018 American Chemical Society. (l) In 2019, Choi *et al.* demonstrated that using compact 2D PC nanodisk array as ETL can greatly enhance light harvesting of PSCs.[92] Reproduced with permission from Choi *et al.*, Nano Energy **56**, 365–372 (2019). Copyright 2019 Authors, licensed under a Creative Commons Attribution (CC BY) license. (m) Nanz *et al.* reported the photon recycling of PCs for PSCs.[93] Reproduced with permission from Nanz *et al.*, APL Photonics **4**, 076104 (2019). Copyright 2019 Authors, licensed under a Creative Commons Attribution (CC BY) license. (n) Zhang *et al.* reported efficient metal halide perovskite LEDs with greatly improved light extraction on nanophotonic substrates.[94] Reproduced with permission from Zhang *et al.*, Nat. Commun. **10**, 727 (2019). Copyright 2019 Authors, licensed under a Creative Commons Attribution (CC BY) license. (o) In 2020, Liu *et al.* prepared color PSCs by using 2D PCs.[95] Reproduced with permission from Liu *et al.*, Nanoscale **12**, 8425–8431 (2020). Copyright 2020 Authors, licensed under a Creative Commons Attribution (CC BY) license. (p) In 2021, Oh *et al.* demonstrated a highly flexible and stable perovskite/microbead hybrid PDs through enhanced interfacial light trapping.[96] Reproduced with permission from Oh *et al.*, Appl. Surf. Sci. **544**, 148850 (2021). Copyright 2021 Authors, licensed under a Creative Commons Attribution (CC BY) license. (q) Wang *et al.* first reported that a kind of encapsulation-enabled perovskite-PMMA film combined with a micro-LED can be used in white-light communication.[97] Reproduced with permission from Wang *et al.*, ACS Appl. Mater. Interfaces **13**(45), 54143–54151 (2021). Copyright 2021 American Chemical Society. (r) In 2022, Daem *et al.* were the first to demonstrate, theoretically and experimentally, the effect of the 3D IO photonic nanostructuration of perovskite photoactive layer in PSCs.[98] Reproduced with permission from Daem *et al.*, ACS Appl. Nano Mater. **5**(9), 13583–13593 (2022). Copyright 2022 American Chemical Society.

II. OPTICAL CHARACTERISTICS OF PHOTONIC CRYSTALS

The concept of PCs dates back to the work by Rayleigh in 1888,[99] who was able to show that multi-layer dielectric stack systems have a one-dimensional PBG, which enables total reflectivity. However, research in the PC field became active first in the 1980s with the introduction by Yablonovitch[72] and John[73] of 2D and 3D PCs consisting of periodic repeated units with different dielectric constants or refractive indices of materials (Schematic 2). A concomitant development of

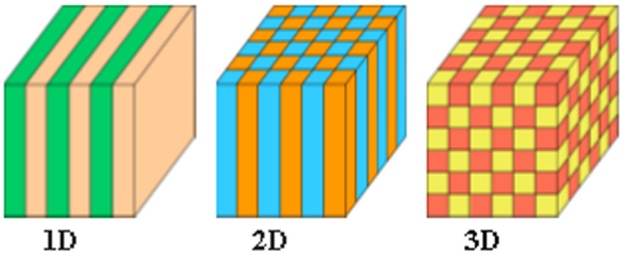

SCHEME 2. Diagrammatic sketch of 1D, 2D, and 3D PCs.

photonic band theory took place, which can be considered as an optical analogue of solid-state electronic band theory. The theory can be employed to calculate the dispersion characteristics of light in various PCs and predicts the existence of a PBG-a unique frequency band for inhibiting optical modes.[100] To generate unique PBGs, the periodicity of PCs should be comparable to the wavelength of photons, in which photon propagation can be precisely controlled as traveling photons through the PCs.[101]

By now, the concept of PCs defines a wide research field within photonics with high potential and also already realized applications, like reflecting laser mirrors, cavity-enhanced light emitting diodes, various types of reflecting coatings, and topological photonics.[102] More spectacular applications, like slowed or fully stopped light and cloaking of objects, are currently extensively researched. The widening of applications has though been hampered by fabrication difficulties, especially for 3D structures and for the optical scales. A 3D PC with a PBG in the microwave region was first established in a transparent material with an array of holes.[103] Semiconductor techniques and materials could later be used to fabricate two-dimensional PCs at optical wavelengths, see, for example, Krauss *et al.*[104] 2D PCs have now matured for commercial applications, in particular in the form of photonic crystal fibers[105] that possess more advanced properties over normal optical fibers. Other important applications of 2D PCs concern optical processing of communication systems where the PCs are etched into integrated computer chips.

Self-assembly principles have been applied to construct PBGs in 3D PCs, based on dielectric spheres that originally are dispersed in solution.[106] The so-called inverse opal structures with a complete PBG can be constructed this way.[74,107] Etching techniques commonly used for 2D PCs have also been applied for 3D constructions, in particular for so-called woodpile structures. Modern techniques including electron-beam lithography, dry etching, sputter deposition, and autocloning applied in sequence or in combination can be used to achieve the sought-after microperiodicity in the materials. Silica and various metal oxides are often used as basic materials. Organic materials have also been tried out to construct 3D photonic materials, for instance, "3D chess boards" consisting of dendritic polymer materials with different dielectric constants. Biomimetic techniques have been used trying to replicate photonic crystals like structures in butterflies and insects.[108]

The basics of PCs can be understood as follows. The macroscopic magnetic field, $\mathbf{H}(\mathbf{r})$, induced by the electromagnetic wave with frequency ω propagating through the medium with dielectric constant $\varepsilon(\mathbf{r})$ can be found as

$$\nabla \times \left(\frac{1}{\varepsilon(r)} \nabla \times \mathbf{H}(\mathbf{r})\right) = \left(\frac{\omega}{c}\right)^2 \mathbf{H}(\mathbf{r}), \tag{1}$$

where c represents the propagation speed of light in vacuum. This equation, together with the requirement of transversality, tells us everything we need to know about the electromagnetic wave propagating through the medium. Notice that the electric component, $\mathbf{E}(\mathbf{r})$, can be found via Maxwell's equations.

A PC is a *periodic* medium, that is, having a dielectric constant $\varepsilon(\mathbf{r}) = \varepsilon(\mathbf{r} + \mathbf{R})$, where $\mathbf{R} = a\hat{\mathbf{e}}_1 + b\hat{\mathbf{e}}_2 + c\hat{\mathbf{e}}_3$ with *a, b,* and *c* being real numbers, and $\hat{\mathbf{e}}_i$ are basis vectors. The basis vectors $\hat{\mathbf{e}}_i$ depend on the dimensions of the PC: two, one, or none of them are zero for 1D, 2D, and 3D PC, respectively. For a periodic medium (and thus for a PC), the solution of Eq. (1) can be written in the form (according to the Bloch–Floquet theorem)

$$\mathbf{H}_{n,\mathbf{k}}(\mathbf{r}) = e^{i\mathbf{k}\cdot\mathbf{r}} \mathbf{u}_{n,\mathbf{k}}(\mathbf{r}), \tag{2}$$

which is a plane wave modulated by a periodic function $\mathbf{u}_{n,\mathbf{k}}(\mathbf{r}) = \mathbf{u}_{n,\mathbf{k}}(\mathbf{r} + \mathbf{R})$. For a given Bloch vector, $\mathbf{k}$, the eigenvalue equation (1) can be solved to yield a collection of nth Bloch mode eigenfunctions $\mathbf{H}_{n,\mathbf{k}}$ and eigenvalues $\omega_n(\mathbf{k})$. When plotted over the reciprocal space, $\omega_n(\mathbf{k})$ form discrete bands, where each band is a continuous function of $\mathbf{k}$. A bandgap occurs at frequencies where no solution exists for any possible Bloch vectors $\mathbf{k}$. Noteworthy, the eigensolutions are also periodic functions of $\mathbf{k}$ in the reciprocal space with the basis vectors $\mathbf{b}_j$ satisfying $\hat{\mathbf{e}}_i \cdot \mathbf{b}_j = 2\pi\delta_{ij}$, where δ_{ij} is the Kronecker delta. Thus, it is necessary only to find solutions for $\mathbf{k}$ vectors within the first Brillouin zone, defined as the region of reciprocal space centered on $\mathbf{k} = 0$ in which any two wave vectors are separated by less than a reciprocal lattice vector. We emphasize that a solution of Eq. (1), being the wave equation, is sufficient for getting eigenfunctions and eigenvalues, and thus for determining the dispersion relation $\omega = \omega_n(\mathbf{k})$. The reason to solve the eigenproblem for magnetic fields instead of electric fields is pure mathematical convenience: the solution of the wave equation for $\mathbf{E}(\mathbf{r})$ is unnecessarily complicated.[101]

Having established the dispersion relation and the electromagnetic field distribution within and near the given PC, one can discover numerous peculiar phenomena such as omnidirectional propagation of light, light trapping, and the enhancement of the spontaneous emission of light. Because of the capability to manipulate light propagation, PCs can be used for performance improvement of perovskite devices from four aspects: (1) constructing PCs as back mirrors to reduce light loss and increase light absorption efficiency; (2) the "slow-photon effect" at the bandgap edge of PCs can boost the coupling between incident photons and perovskite materials, resulting in the improvement of excitation/emission efficiency; (3) PCs can serve as scattering layers to enlarge the propagation distance of light in the perovskite material, improving the absorption efficiency by producing resonance enhancement mode; and (4) due to the large specific surface areas, especially for three-dimensional PCs, they can be used as supporters for substantially increasing the loading capacity and activity of perovskite materials. Below we discuss in detail how these aspects are used in perovskite devices.

III. PC MODULATION OF LIGHT ABSORPTION AND SPONTANEOUS EMISSION OF PEROVSKITE MATERIALS

Recently, significant advances have taken place for the controlled modulation of spontaneous emission in various quantum systems by PCs (e.g., fluorescent dyes, quantum dots, 2D NCs, and upconversion NCs).[109–112] These achievements apply equally to perovskite luminescent materials. The first example using 1D PCs was demonstrated by Lova *et al.* in 2018[113] and further developed for 2D and 3D PCs. In this section, we will review the luminescent modulation of perovskite materials through PCs.

A. Theoretical description

As is well known, the emission intensity of as-prepared perovskite materials can be expressed by the equation as follows:[114,115]

$$I = I_{\text{exc}}\eta_{\text{int}}\eta_{\text{ext}}, \tag{3}$$

where I_{exc} represents the incident excitation optical field intensity, η_{int} shows photo-luminescent internal quantum efficiency, and η_{ext} is the extracted efficiency of emission light. The internal quantum efficiency of perovskite materials can be calculated according to the equation

$$\eta_{\text{int}} = \frac{\gamma_{\text{rad}}}{\gamma_{\text{rad}} + \gamma_{\text{nrad}}}, \tag{4}$$

where γ_{rad} and γ_{nrad} are radiative and nonradiative rates, respectively.

According to Fermi's golden rule, the radiative transition rate is directly impacted by the density of states of photon modes, and γ_{rad} is determined by the following equation:[116]

$$\gamma_{\text{rad}} \propto \frac{2\pi}{h}\left|M_T(E_{21})\right|^2 p_r(E_{21})p_0(\nu_{21}), \tag{5}$$

where $M_T(E_{21})$ refers to the transition matrix element over the electronic wave functions under a given electromagnetic field. $p_r(E_{21})$ and $p_0(\nu_{21})$ are the electronic and photonic density of states. The local density of states in a PC is in charge of altering the dipolar spontaneous transition rates. The spatial distribution of the emitters and the number of optical modes in a PC should be precisely manipulated to realize regulation of spontaneous emission of perovskite materials.

The local density of electromagnetic states within PC bandgaps can decrease or entirely vanish in all directions or in a specific direction, but will increase at the bandgap edge. This feature depends on the type of crystal structure and the contrast between the dielectric constant of the crystal and its surroundings. In addition, the local densities of electromagnetic states change with position as a result of variation of the refractive index. Therefore, emitters occupying different positions will exhibit different luminescence properties. In this regard, PCs with bandgaps are exciting alternatives for manipulating the photon emission characteristics of internal light. Many previous reports have demonstrated that PCs possess the capability to effectively control the light propagation of emitters.

The altered emission can be approximately described by the Purcell factor, which refers to that the spontaneous emission rate of a light source can be increased over its bulk value when a system is coupled to a resonant cavity

$$F_P = \frac{\gamma_{\text{PC}}}{\gamma_0}, \tag{6}$$

where γ_0 and γ_{PC} denote the respective total rates without or with the presence of a PC.

In addition, the two optical modes exist inside a perovskite film, including guided modes and vertical modes. By virtue of the high refractive index of perovskite materials, light emission confines inside the perovskite material by the guided modes. In the contrast to the guided modes, the vertical modes lead to penetrate the perovskite films, thus increasing the extraction efficiency. Spontaneous emission light of perovskite films can be coupled into both guided modes and vertical modes. Based on the above, only the vertical modes have positive contribution to useful luminescence, but the guided modes usually cause loss and noise. Therefore, the total spontaneous emission rate (γ_{tot}) can be given by

$$\gamma_{\text{tot}} = \gamma_{\text{guid}} + \gamma_{\text{vert}}, \tag{7}$$

where γ_{guid} and γ_{vert} refer to the light emission rates in the form of guided and vertical modes, respectively. Generally, the emission is strongly limited and confined inside the space of the perovskite films ($\gamma_{\text{guid}} \gg \gamma_{\text{vert}}$) when perovskite films are surrounded by low refractive index of materials (e.g., air), lowing extraction efficiency. However, the guided modes in the perovskite films can be significantly inhibited by reducing emission rate when the emission wavelength overlaps with the PBG in a perovskite/PC hybrid. Meanwhile, most of the light emission is redistributed into vertical modes, leading to the improved extraction efficiency.

Generally, when integrating perovskite materials with PCs, the I_{exc}, η_{int}, and η_{ext} quantities can be altered, leading to modified luminescent properties. Therefore, the fluorescence enhancement or reduction can be expressed as follows:

$$AFs = AF_{\text{exc}} \times AF_{\text{em}} \times AF_{\text{ext}} = \frac{|E_{\text{PC}}|^2}{|E_0|^2} \times \frac{\eta_{\text{int;PC}}}{\eta_{\text{int;0}}} \times \frac{\eta_{\text{ext;PC}}}{\eta_{\text{ext;0}}}, \tag{8}$$

where AF_{exc} and AF_{em} refer to the excitation and emission altered factors, and E_0 and E_{PC} are the electric field intensity without/with the PC. $\eta_{\text{int;0}}$ and $\eta_{\text{int;PC}}$ present the internal quantum efficiency of perovskite materials without or with PC. $\eta_{\text{ext;0}}$ and $\eta_{\text{ext;PC}}$ is the extraction efficiency without/with the PC. It is obvious that the fluorescence enhancement is proportional to the altered excitation field, the quantum efficiency, and the extraction efficiency.

B. Luminescent enhancement of perovskite by PCs

1. Perovskite materials in the front of 1D PCs

The spontaneous emission of perovskite materials can be easily modified by altering the photonic environment surrounding it. The most often used strategies to achieve such task by employing various photonic structures, for example, distributed Bragg reflectors (DBRs) and microcavities, which can realize the spectral and directional redistributions of spontaneous emission of luminescent materials. Lova *et al.*[113] first demonstrated in 2018 the coupling of broad-emitting 2D perovskites (2,2-(ethylenedioxy)bis(ethylammonium)$PbCl_4$) with a DBR. The DBR consisted of polystyrene (n = 1.58) and cellulose acetate (n = 1.46) with different reflective indices with controllable PBG within 400–600 nm, overlapping with the emission of the above 2D

perovskites. Obviously, the typical emission suppression within the PBG region in the back configuration and enhancement at the long wavelength side of the PBG in the front configuration were recorded through the PBG effect [Fig. 1(a)].

2. Perovskite emitters as 2D PCs

Apart from positioning a 1D PC layer on top or back side of the emitting layer, perovskite light emitters can serve as PCs themselves. For example, Hou *et al.*[67] in 2019 fabricated PCs directly on all inorganic perovskite films by combing techniques of electron beam lithography (EBL) and reactive ion etching (RIE). They demonstrated the first simultaneous emission rate inhibition and enhanced light extraction in $CsPbBr_{2.75}I_{0.25}$ 2D PCs. They observed a significant increase in lifetimes with the reduction of the spontaneous emission rate (7.9-fold) and PL emission enhancement of 23.5-fold in $CsPbBr_{2.75}I_{0.25}$ 2D PCs. These were assigned to light emission redistribution from guided modes to vertical modes in perovskite PCs thin films by the engineering of the PBG effect [Fig. 1(b)]. Similarly, in 2020 Park *et al.*[117] fabricated nanocylinder- and nanocone-patterned $CsPbBr_3$-SiO_2 films through a soft imprint lithography technique, resulting in 3.71- and 4.62-fold PL enhancement compared with the planar counterpart. The improvement of the PL properties of the $CsPbBr_3$ PNCs could have originated from the enhanced light absorption induced by Mie-scattering and spontaneous emission produced by the Purcell enhancement within the nanostructures. Meanwhile, the $CsPbBr_3$–SiO_2 films exhibit improved heat and water stability.

3. Perovskite emitters on the top surface of 3D PCs

In 2009, Susumu Noda experimentally evidenced that 3D PCs are capable of controlling and manipulating photons when placing perovskite emitters on the surface of a 3D PC. They demonstrated that 2D surface states on the surface of 3D PCs can confine and propagate the photons.[118] A lot of works reported in the literature have employed 2D surface states in 3D PCs to improve the luminescence of various emitters, such as fluorescent dyes, quantum dots, carbon dots, and upconversion NCs.[109–112] Our group[77] assembled blue perovskite colloidal nanocrystals ($CsPbCl_3$ NCs, with the thickness of 50 nm) on the top surface of 3D polymethyl methacrylate (PMMA) PCs. Compared to the $CsPbCl_3$ NCs on the glass substrate, an optimized enhancement of 20 folds was recorded for the $CsPbCl_3$ NCs as the PBG of the PCs matched well with the emission wavelength of the $CsPbCl_3$ NCs, which involves the excitation enhancement (∼4.1-fold) and Purcell enhancement (∼4.5-fold) when the $CsPbCl_3$ NCs and PMMA PCs are coupled. Localized optical manipulation by surface plasmon resonances is a promising approach to improve PL when the emitters are close to plasmonic structures. We further coupled a 3D PC with a plasmonic structure (Ag nanoparticles) to boost the luminescence of $CsPbCl_3$ NCs for the first time. Through cascade optical field amplification of

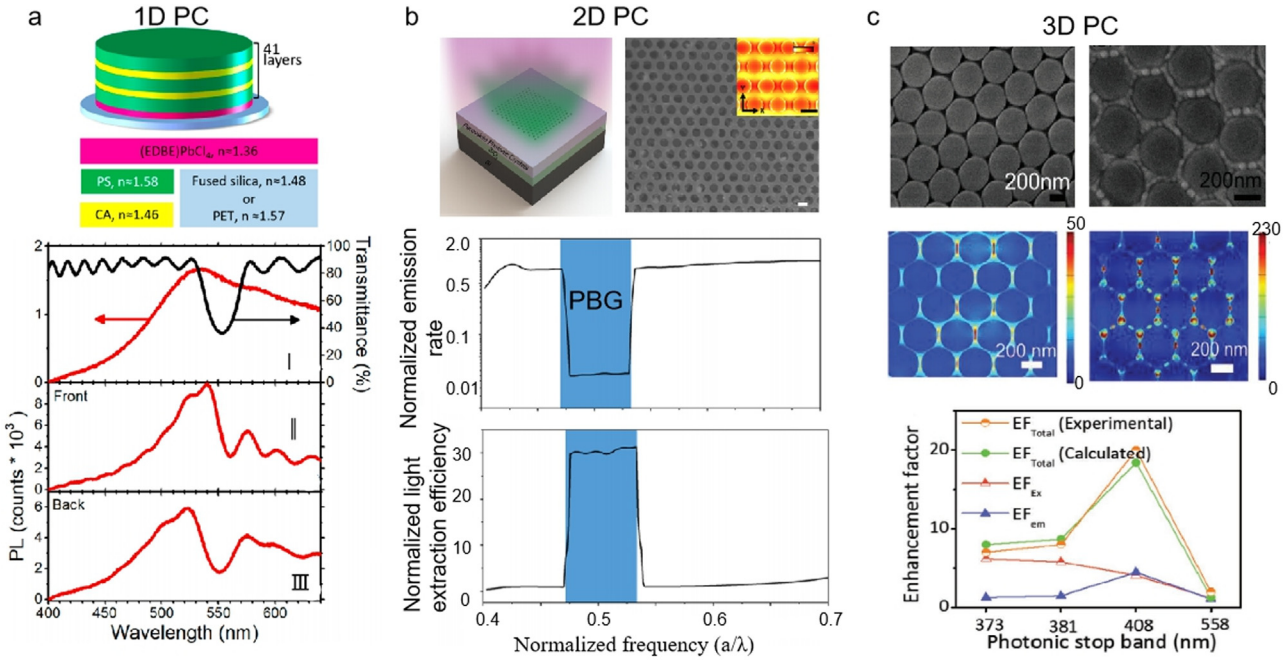

FIG. 1. PC for luminescent modulation of perovskite materials: (a) Schematic of the $(EDBE)PbCl_4$ DBR, transmittance spectrum of an $(EDBE)PbCl_4$ DBR with PBG centering at 560 nm (black line) and PL spectrum of $(EDBE)PbCl_4$ film (red line, |), and PL emission intensity of $(EDBE)PbCl_4$ DBR [front (||) and back (III)]. Reproduced with permission from Lova *et al.*, ACS Photonics **5**, 867–874 (2018). Copyright 2019 American Chemical Society.[113] (b) Schematic, scanning electron microscope (SEM) image, and calculated the spontaneous light emission rate and light extraction efficiency in the vertical direction of a 2D perovskite PC. Scan bar is 200 nm. Reproduced with permission from Hou *et al.*, ACS Photonics **6**, 1331–1337 (2019). Copyright 2019 American Chemical Society.[67] (c) SEM images (top) and simulated electric field intensity distribution (middle) of PMMA OPCs and Ag/PMMA OPCs films; calculated and experimental enhancement factors (EFs), calculated excitation enhancement (EF_{Ex}) and the emission enhancement (EF_{Em}) of $CsPbCl_3$/OPCs with different PSBs. Adapted with permission from Li *et al.*, Adv. Mater. **28**, 1804429 (2018). Copyright 2018 Authors, licensed under a Creative Commons Attribution (CC BY) license.[77]

surface plasmon and PC effects, the PL emission intensity of the $CsPbCl_3$ NCs was enhanced ∼150-fold with an emission efficiency of ∼51.5% [Fig. 1(c)].[77] Wang *et al.*[119] reported full-color polarized light emission from inorganic $CsPbX_3$ perovskite NCs when embedded in predefined handedness cholesteric superstructure stacks. They serve as filters to transform the unpolarized light emission of the perovskite NCs into angular dependence of the circularly polarized luminescence.

IV. ENHANCING THE LIGHT-EMISSION EFFICIENCY OF LEDS

The next-generation LEDs not only require high efficiency, high color quality, and adjustability, but also require low energetic and economic costs of manufacturing.[120] Although inorganic LEDs have been commercialized and shown effective in saving energy, the preparation of III-V semiconductor materials requires high temperature and strict vacuum-based processing with epitaxial growth on expensive rigid substrates. As the best alternative to inorganic LED, organic LEDs (OLEDs) and colloidal quantum dots LEDs (QLEDs) have attracted much attention,[121,122] However, the high surface-defect concentration of QLEDs infers strong non-radiative recombination. Apart from that, the OLEDs based on vacuum sublimation are also unsuitable for cost-effective fabrication of large-area devices. The above-mentioned limitation has not been observed in perovskite materials due to their low-temperature solution processing, direct bandgap, and low defect densities.[123,124] Furthermore, perovskite LEDs have made great progress with EQEs of up to ∼22% for green emission, matching that of well-developed OLEDs.[125,126] While PL quantum efficiencies of visible LEDs reach close to ∼100%, in practice, the emitted light radiated in vertical directions is only $\approx 1/4n^2$ (n is the refractive index of the luminescent films) of LEDs. Thus, most of the photons can be trapped and eventually be re-absorbed in the films, by virtue of the contribution of guided modes within them. Thus, the emitted light extracted from the top surface of the devices occupies only a small proportion (≈5%). Considering the significance of light extraction, great efforts should be paid toward designing of novel and efficient light extracting structures. The use of PCs offers the possibility to control and improve light extraction efficiencies in LEDs.[78] Experimentally, Zhang *et al.*[94] fabricated methylammonium lead bromide LEDs on anodic alumina membranes/titanium dioxide (AAM/TiO_2) PC substrates, consisting of a nanodome array and a nanowire array. An optimal EQE of ∼17.5% in $MAPbBr_3$/PC device was achieved, which enhanced two times than that of the planar device without PC. Theoretical modeling estimated that $MAPbBr_3$/PC device had a light extraction efficiency of ∼73.6%. The EQE enhancement is attributed to two aspects: the nanodome array serving as light couplers to couple more light into nanowire array of the PCs; subsequently, the nanowire arrays work as antennas to transform confined energy from guided modes to leaky modes, resulting in enhancement of light extraction efficiency in perovskite LEDs. [Figs. 2(a) and 2(b)].

As mentioned above, because of the difference of refractive index between perovskite materials and injection layers in devices (refractive index of perovskite materials is larger than of injection layers), a large portion of the generated light of perovskite LEDs is confined in guide modes in the perovskite film, which reduces the light extraction efficiency. The recent successes of achieving high EQE (> 20%) perovskite LEDs have been widely reported. To explain such phenomenon, the photon recycling (PR) processes should be carefully considered for the perovskite LEDs. The outcoupling efficiency of LEDs can be estimated through integral of the recursive photon recycling (PR) processes. Therefore, the external photoluminescence quantum efficiency (PLQE) (η_{ext}) can be expressed as a series over multiple re-absorption events[127]

$$\begin{aligned}\eta_{ext} &= \eta_{esc}\cdot\eta_{int} + \eta_{esc}\cdot(1-\eta_{esc})\cdot\eta_{int}^2 \\ &\quad + \eta_{esc}\cdot(1-\eta_{esc})^2\cdot\eta_{int}^3 +, \ldots, \\ &= \eta_{esc}\cdot\eta_{int}\cdot\sum_{k=0}^{\infty}(1-\eta_{esc})^k\cdot\eta_{int}^k, \\ &= \frac{\eta_{int}\cdot\eta_{esc}}{1-\eta_{int}+\eta_{int}\cdot\eta_{esc}}. \end{aligned} \tag{9}$$

η_{esc} is here the photon escape probabilities from the perovskite film. Cho *et al.*[78] theoretically analyzed the influence of photon recycling (PR) on perfecting light extraction from perovskite LEDs and demonstrated that the sufficiently high emission efficiency is prone to largely boost the light extraction through repeating re-absorption and re-emission of photons confined in the substrate and waveguide modes. About a proportion of ∼70% of the overall emission was contributed by the PR process. In addition, they pointed out that PR process may lead to an outcoupling efficiency of 100% theoretically, but inevitable absorption losses originating from absorption by the electrodes limited the practical efficiency in such device. This study[78] explains the recent success of obtaining high EQE (>20%) perovskite LEDs through manipulating light extraction efficiency [Fig. 2(c)]. Wu *et al.* used "sandwich" $CsPbX_3$ (X = Cl, Br, and I) perovskite QDs/inverse opal PC composites to obtain white LEDs.[128] The non-wetting of inverse opal PCs structures can prevent the exposure of perovskite QDs exposure to air and contact with water, leading to the enhanced luminescence stability for more than four months. Meanwhile, the inverse opal PCs have larger inner surface areas for dispersing perovskite QDs, which can avoid the fluorescence quenching caused by the agglomeration of the perovskite QDs. In addition, polymethyl methacrylate (PMMA) can also be employed for wrapping and dispersing perovskite nanocrystals (PNCs), in order to enhance the air stability of the perovskite QDs. In 2021, Wang *et al.* fabricated PNC-PMMA films with red and yellow emission on the GaN-based blue micro-LED (μLED) with 75 μm diameter, which was constructed for Vis light communication.[97] This color-converted PNC-PMMA films can realize color rendering index and correlated color temperature of, respectively, 75.7 and 5670 K, as well as achieve modulation bandwidths of 347 and 822 MHz.

V. PCS FOR PEROVSKITE LASERS

Laser threshold is defined as the lowest energy density for laser oscillation, which is a crucial index for laser device integration. Compared with other semiconductor materials (ZnO, GaAs, and GaN), perovskite is an ideal gain material for low-threshold lasers due to their high optical gain. Quantum confined systems from lower-dimensional layered perovskite materials combined with nanostructures realize a low-threshold or even no-threshold pump laser in the form of a PC.[69,120] Apart from that, solution-processed perovskites have emerged as a prospect gain media for semiconductor lasers owing to their large absorption coefficient, high photoluminescent efficiency, and facile synthesis. Stimulated radiation from perovskites has been presented in the form of random lasers,[129] whispering-gallery mode

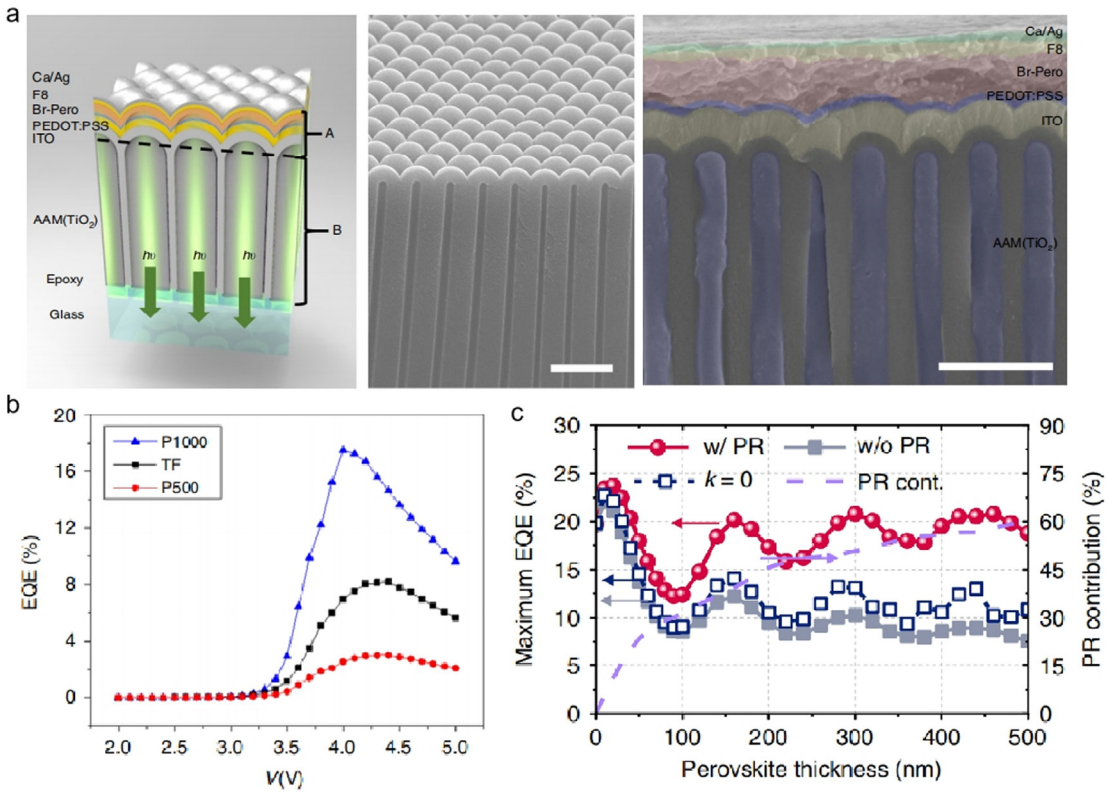

FIG. 2. Light-emission efficiency and photon recycling processes of perovskite LEDs. (a) Device on nanophotonic substrate, cross-sectional SEM images of free-standing AAM film, and a perovskite LED integrating with AAM. Scale bars are 1 μm. (b) EQEs of the thin films without/with AAM structures. Adapted with permission from Choi *et al.*, Nano Energy **56**, 365–372 (2019). Copyright 2019 Author(s);[91] Adapted with permission from Zhang *et al.*, Nat. Commun. **10**, 727 (2019). Copyright 2019 Authors, licensed under a Creative Commons Attribution (CC BY) license. (c) The influence of parameters on calculated EQEs: with PR, without PR, without re-absorption, and PR contribution for an ideal perovskite LED as a function of perovskite thicknesses. Adapted with permission from Cho *et al.*, Nat. Commun. **11**, 611 (2020). Copyright 2020 Authors, licensed under a Creative Commons Attribution (CC BY) license.[78]

laser,[130] and in vertical-cavity configurations using multilayer dielectric and gold reflectors.[131,132] Integrating perovskite within or on the surface PC nanostructures can effectively decrease the pumping threshold of lasing, and achieve a high degree of temporally and spatially coherent lasing.

A. Perovskite lasers as 1D PCs

In 2018, Li and his coauthors[133] demonstrated room-temperature lasing behavior in a distributed feedback $MAPbI_3$ perovskite resonator (similar to those of a grating) on a silicon substrate under continuous-wave optical pumping with the ultralow lasing threshold of 13 W/cm^2. Such high performance was attributed to the direct patterning of perovskite by thermal nanoimprint lithography (NIL), in which a high-Q-factor cavity with large mode gain was formed, as well as the emission properties of perovskite was enhanced [Fig. 3(a)].

B. Perovskite lasers on top of 2D PCs.

Perovskite QDs have a large two-photon absorption cross section reaching up to 2×10^5 GM, simulating the applications on low-threshold stimulated emission and lasing under multiphoton pumped, whereas multiphoton absorption involving the participating of virtual energy levels is usually weak contrast to single-photon processes, which satisfies with the *n*th power of the excitation intensity (n is the number of absorbed photons). Becker *et al.*[134] investigated two-photon pumped photoluminescence of $CsPbBr_3$ perovskite QDs (9.4 nm) on a silicon PC slab. An enhancement of more than one order of magnitude was observed under the two-photon excitation of 925 and 972 nm, which was assigned to near-field enhancement effects of photonic leaky modes of the 2D PC slab [Fig. 3(b)]. Chen *et al.*[87] developed a perovskite laser embedded within a 2D PC resonator through electron beam deposition. A temporally and spatially coherent lasing with well-defined directional emission was achieved around 788 nm wavelength at a pumping threshold of 68.5 ± 3.0 μJ/cm^2. It was ascribed to the formation of high-quality $CH_3NH_3PbI_3$ densely packed films with an enhancement of the photon confinement and light trapping in the 2D PC nanostructure resonators [Fig. 3(c)].

C. Perovskite lasers as 2D PCs

Pourdavoud *et al.*[135] demonstrated organo-metal halide perovskite 2D PC lasers patterned via thermal nanoimprint lithography,

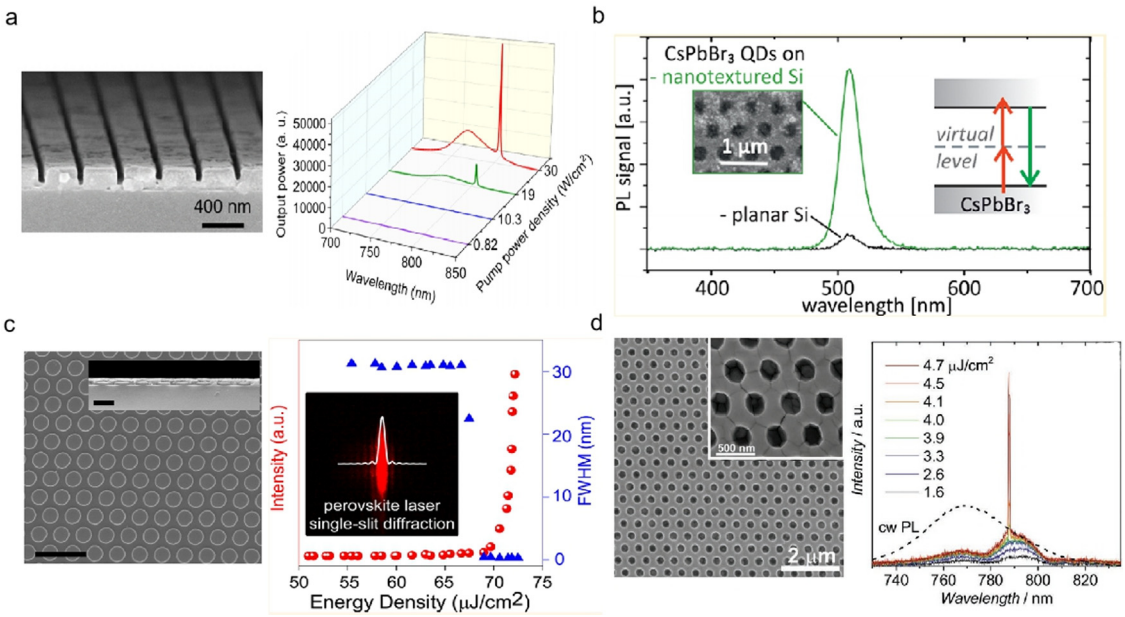

FIG. 3. Perovskite lasers based on 1D-2D PCs. (a) Perspective view SEM image and output power of the lasing wavelength of the imprinted $MAPbI_3$ DFB resonator depending on the pump power density. Reproduced with permission from Li *et al.*, ACS Nano **12**, 10968–10976 (2018). Copyright 2018 American Chemical Society.[133] (b) Emission spectra of $CsPbBr_3$ QDs on silicon nanohole array layer or planar silicon at the excitation of 925 nm. Inset shows SEM image of the silicon nanohole array layer on glass substrate with drop-cast $CsPbBr_3$ QDs, and the energy-level diagram of excitation and emission of the two-photon absorption. Reproduced with permission from Becker *et al.*, ACS Photonics **5**, 4668–4676 (2018). Copyright 2018 American Chemical Society.[134] (c) Left: SEM image of a 2D PC (the scale bar is 1 μm). Inset shows cross-sectional SEM image of perovskite film on a 2D PC pattern. Right: Pumping threshold and full width at half maxima of the perovskite PC depending on excitation power density. Inset highlights the sharp threshold by the same plot on a logarithmic scale.. Reproduced with permission from Chen *et al.*, ACS Nano **10**, 3959–3967 (2016). Copyright 2016 American Chemical Society.[87] (d) SEM of the imprinted $MAPbI_3$ perovskite layer (inset: magnified view), and emission spectra upon optical pumping with increasing energy density 1.6–4.7 μJ cm^{-2}. Adapted with permission from Pourdavoud *et al.*, Adv. Mater. **29**, 1605003 (2017). Copyright 2017 Authors, licensed under a Creative Commons Attribution (CC BY) license.[135]

which significantly smoothened and reduced surface defects compared to the pristine polycrystalline perovskite layer with an increased optical density of states at the photonic band edges. The 2D-PC lasers operated with the low lasing thresholds of 3.8 μJ cm^{-2}, lower than the recently reported lasing threshold (68.5 μJ cm^{-2}) for a laser, where the perovskite layer has been deposited on top of a 2D-PC substrate [Fig. 3(d)].

D. Perovskite lasers inserted in 3D PCs

Song's group achieved a narrow and low-threshold amplified spontaneous emission in 3D perovskite PCs, fabricated through a typical solvent method using an opal template.[136] The 3D perovskite PCs afforded stimulated radiation with a threshold of 35.5 mJ cm^{-2}, assigned to the strong coherent scattering and the high-intensity resonance fields in the 3D PCs [Fig. 4(a)]. Mikosch *et al.*[137] demonstrated a perovskite/conjugated polymer hybrid material by integrating a methylammonium lead-halide perovskite matrix $CH_3NH_3Pb(Br_xCl(_{1-x}))_3$ with monodisperse poly(fluorene-co-divinylbenzene) particles (MPP), which was self-assembled into a PC forming an inorganic matrix in the interstitial space. Laser emission at fluences of 13 mJ/cm^2 was obtained due to energy transfer from the perovskite to the self-assembled MPP PC. It can be seen that the perovskite serves both as an encapsulating matrix assisting ordering of the particles and as a donor, promoting laser emission of the MPPs. The nonradiative energy transfer efficiency from the perovskite to the particle was enhanced by 37% by controlling the spectral overlap of the perovskite emission energy with the absorption of the particles [Fig. 4(b)].

E. Perovskite lasers as 3D inverse PCs

Chen *et al.*[138] achieved the lasing emission of 3D distributed feedback perovskite, which was fabricated via a colloidal crystal templating approach without the use of expensive and elaborate lithography techniques. The as-prepared $CH_3NH_3PbBr_3$ films with inverse opal morphology displayed lasing emissions with a full-width half-maximum of 0.15 nm and good long-term stability under pulsed laser excitation above the lasing threshold of 1.6 mJ cm^{-2} [Fig. 4(c)].

F. Chiral nematic liquid crystals (CLCs).

A liquid crystalline phase formed by chiral nematic liquid crystals (CLCs) can spontaneously self-assemble to a macroscopic helicoidal structure.[139] Similarly to PC, when the length scale defining the periodicity of the CLC helix is on the order of the wavelength of light, Bragg reflection can be clearly observed. Stranks *et al.*[82] sandwiched a $CH_3NH_3PbI_3$ perovskite thin film with 50 nm thickness within a cavity

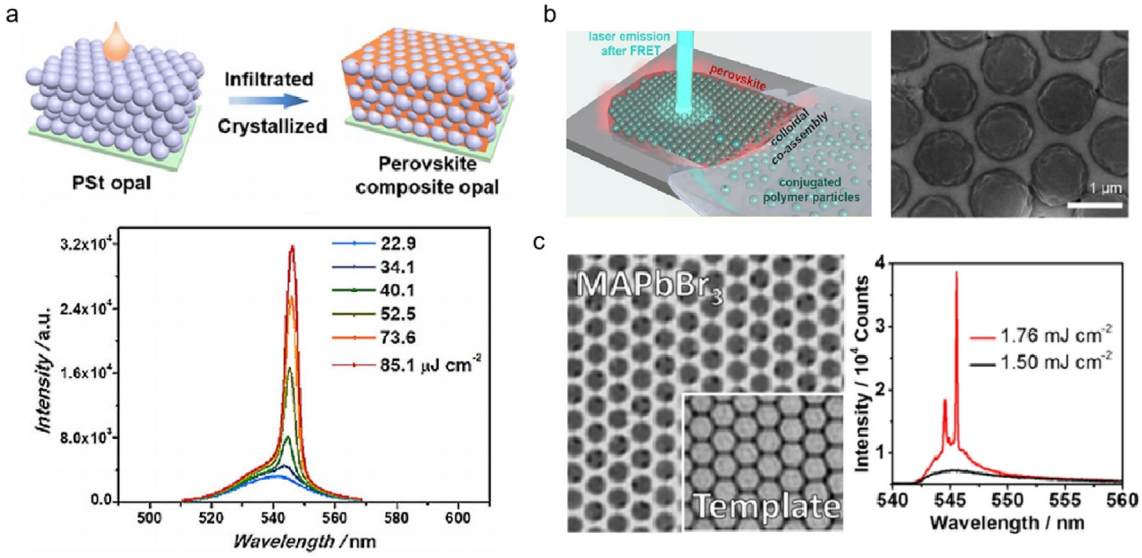

FIG. 4. 3D PCs for perovskite lasers. (a) Schematic preparation process and power dependence of emission spectra of 3D perovskite OPCs. Adapted with permission from Zhou *et al.*, ChemPhysChem **19**, 2101–2106 (2018). Copyright 2018 Authors, licensed under a Creative Commons Attribution (CC BY) license.[136] (b) Schematic of laser emission and SEM image by integrating conjugated polymer particles with a perovskite matrix. Reproduced with permission from Mikosch *et al.*, Chem. Mater. **31**, 2590–2596 (2019). Copyright 2019 American Chemical Society.[137] (c) SEM images of $MAPbBr_3$ perovskite inverse opal PCs and polystyrene beads template, and emission spectra at the excitation power density of 1.50 and 1.76 mJ/cm^2, respectively. Reproduced with permission from Schünemann *et al.*, ACS Photonics **4**, 2522–2528 (2017). Copyright 2017 American Chemical Society.[138]

composed of a CLC reflector ($\sim 7\,\mu$m) and a metal back-reflector. They recorded optically pumped amplified spontaneous emission at 780 nm, in which the threshold is lower by two orders of magnitude contrast to perovskite films without the CLC layer. They assigned this to improved coupling of the oblique and out-of-plane modes that are reflected into the bulk in addition to any contributions from cavity modes (Fig. 5). Chen *et al.*[140] incorporated lead-free cesium tin halide perovskite quantum dots into the CLC lasing cavities. The lasers exhibit lasing features of low threshold (150 nJ/pulse) and narrow linewidth (0.20 nm), assigned to the combination effects from the suppression of emission loss induced by the quantum confinement of the perovskite quantum dots and the enhanced emission induced by the band edge effect of the CLC.

VI. PCS FOR PSCS

Kojima *et al.*[44] have developed PSCs since 2009, the first ones with the initial the power PCE of 3.8%, achieved an amazing 25% in ten years.[59] Various approaches were implemented to boost the efficiency and/or stability of PSCs, for example, interface engineering,[12,141] ion doping,[17,142] passivation,[143,144] and light management.[145,146] PCs have the ability to enhance light trapping, reduce photon recycling, improve the stability, and construct colorful PSCs. Moreover, PCs can used as back mirrors placed on the outer side of the Si SC opposite electrode,[147] in dye-sensitized solar cells (DSSCs) or in QD-sensitized solar cells (QDSSCs).[148–150] The PC with bandgap in the infrared range is beneficial to boost the performance of Si SCs. Meanwhile, the introduction of PCs can efficiently decrease the fabrication costs as well as the thickness of the Si SCs. However, with Si SCs, it is difficult to realize flexible devices. Noteworthy, PCs are more widely utilized in QDSSCs and DSSCs rather than PSCs. The reason is the limitations of preparation technology and structure of PC, which is difficult to meet the thickness requirements of PSCs.[151]

A. Light trapping enhancement by PCs for PSCs

Improvement of light-harvesting efficiency of PSCs by employing PCs is a promising way to improve their performance.[152] Taking a 1D PC as an example, a typical |gold/spiro-OMeTAD|$CH_3NH_3PbI_3$|PC|ITO| structure appears as displayed in Fig. 6(a). The structure of a TiO_2|SiO_2 nanoparticle multilayer consisting of 1D PC served as a reflector to re-couple the unabsorbed light into the perovskite $CH_3NH_3PbI_3$ layer. The generalized transfer matrix approach was used to reveal the performance of PSCs when coupling the multilayer 1D PC with PSC. The reflection (R) and transmission (T) coefficients within each layer of PSCs can be used to calculate the absorbance (A) or light-harvesting efficiency (LHE), determined by the following equation:

$$\mathrm{LHE} = \mathrm{A} = 1 - \mathrm{R} - \mathrm{T}, \tag{10}$$

where LHE significantly influences the incident power conversion efficiency (IPCE) of PSCs, expressed by the given equation:

$$\mathrm{IPCE}(\lambda) = \eta_{\mathrm{inj}}(\lambda)\eta_{\mathrm{col}}(\lambda)\mathrm{LHE}(\lambda), \tag{11}$$

where $\eta_{\mathrm{inj}}(\lambda)$ and $\eta_{\mathrm{col}}(\lambda)$ refer to the quantum yield of charge injection and the charge collecting efficiency by the photo-anode. The later one is considered to be weakly dependent on the wavelength assumed to be constant ($\sim$1). The short-circuit current density (J_{SC}) of PSC is the

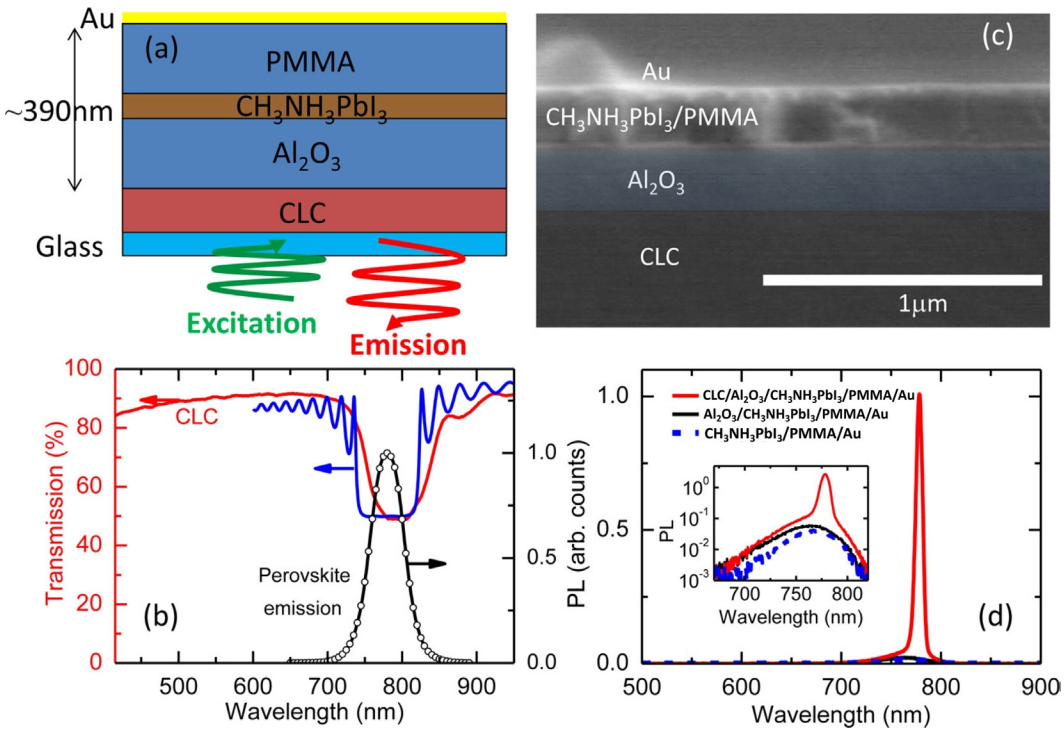

FIG. 5. CLC-based perovskite lasers. (a) Schematic of a CLC device. (b) Transmission spectra of the CLC reflector on glass (red line for experimental transmission spectrum, left axis; blue line for modeled transmission spectrum) with emission spectrum from the perovskite thin film (black circles, right axis). (c) Cross-sectional SEM image of a device structure. (d) Emission from full device stack (red), stack without CLC (black), and stack without CLC and alumina (blue dashed) under the pulsed excitation (530 nm, 4 ns pulses, 10-Hz repetition rate, and ~60 μJ/cm^2/pulse). Reproduced with permission from Stranks *et al.*, Nano Lett. **15**, 4935–4941 (2015). Copyright 2015 American Chemical Society.[82]

integration on the product of spectral photon flux irradiation on the PSC and IPCE as follows:

$$J_{SC} = \int q \cdot IPCE(\lambda) \cdot F(\lambda) d\lambda = \int q \cdot LHE(\lambda) \cdot \eta_{inj}(\lambda) \cdot \eta_{col}(\lambda) \cdot F(\lambda) d\lambda, \quad (12)$$

where the incident photon flux of $F(\lambda)$ presents the ratio between the AM 1.5 solar spectral irradiance and photon energy. q represents the electron charge. When coupling a 1D PC with a PSC, the short-circuit photocurrent density enhances, and the increment (ΔJ_{SC}) can be calculated by the given expression

$$\Delta J_{SC} = \frac{\int [LHE_{PC}(\lambda)] F(\lambda) d\lambda - \int [LHE_0(\lambda)] F(\lambda) d\lambda}{\int [LHE_0(\lambda)] F(\lambda) d\lambda}, \quad (13)$$

where LHE_{PC} and LHE_0 represent the LHE of the PSC integrated with/without a 1D PC, respectively.

Singh *et al.*[152] presented a detailed theoretical demonstration of $CH_3NH_3PbI_3$ PSCs integrated with 1D PCs. The 1D PCs consisted of a TiO_2/SiO_2 nanoparticle multilayer with controllable PBG from 500 to 800 nm with different lattice parameters. The 1D PCs serve as light reflection layers in the PSCs, contributing to the increase in both LHE and photocurrent density (Fig. 6). Sun *et al.*[153] used finite-difference time-domain (FDTD) simulations on different experimentally realistic structures of PSCs (cylindrical nanopillar and nanohole) and optimized their parameters with assistance of a neural network algorithm. An optimized structure showed 30.48% enhancement compared to the planar structure and with a proper design a 300-nm-thick nanotextured structure was shown to outperform a 900-nm-thick planar structure.

B. Experimentally improved light-harvesting efficiency of PSCs by 1D-3D PCs

1. 1D PC

The device processing (e.g., patterning) for organic–inorganic hybrid perovskites is challenging, owing to the sensitivity of organic moieties to solvents and temperature. Alias *et al.*[83] employed the chemically gas-assisted focused-ion beam etching technique to directly pattern $CH_3NH_3PbBr_3$ perovskites using XeF_2 and I_2 as precursors. A perovskite film with high (>90%) and broadband absorption (400–1100 nm) was fabricated, owing to the uniform and periodic structure of submicron subwavelength grating (SWG). They observed an enhancement of light absorption (>20%) of the perovskite materials and device efficiency by integrating with the SWG absorber, which is assigned to the increase in light trapping and absorption by SWG absorber. Jin-Hyo Boo and his coauthors[154] adopted hemisphere TiO_2

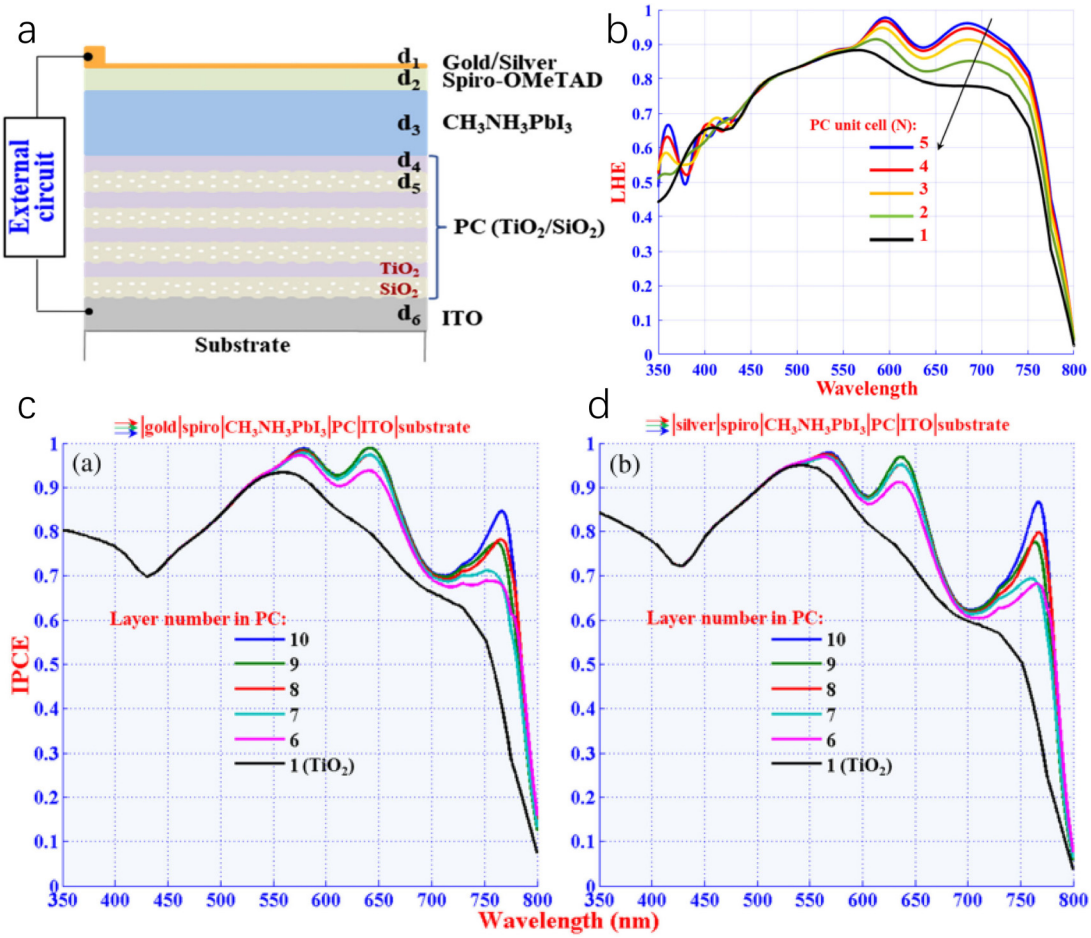

FIG. 6. Theoretical description of PSCs integrated with 1D PCs. (a) Schematic of a PSC integrated with a 1D PC. (b) LHE in the perovskite layer as a function of different numbers of unit cells (N) of 1D PC. (c) IPCE of the PSCs with various numbers of layers of 1D PC for gold and silver as electrodes. Reproduced with permission from Singh *et al.*, Appl. Opt. **58**, 8046–8054 (2019). Copyright 2019 Optica.[152]

PCs and employed the polystyrene beads template as electron transport layer in a PSC. The power conversion efficiency of the PSC was largely enhanced from 10.5% to 15.2%, which could be assigned to the higher light utilization efficiency. Furthermore, the micro-nanophotonic imprinting technique can be used to construct various optical structures. Motivated by this fact, Yanlin Song's group[155] fabricated a perovskite-active layer with a large area grating structure in PSC through using commercial optical disks (CD-R and DVD-R). The first-order diffraction appeared when the perovskite grating with period 0.7–0.8 μm, which enhances the light absorption and effectively suppresses carrier recombination for enhancing power conversion efficiency. Compared with the pristine PSCs, the grating perovskite devices give higher power conversion efficiency from 16.71% to 19.71%, higher photocurrent density from 21.67 to 23.11 mA cm^{-2}, and better stability [Fig. 7(a)]. Similarly, a grating of methylammonium lead iodide perovskite was explored by Massimo Tormen by means of ultrafast nano-imprinting lithography.[156] Hörantner *et al.*[157] demonstrated a double templating approach to fabricate highly ordered patterns metal oxide scaffolds (TiO_2 or SiO_2), which can pattern perovskite thin films. A sacrificial template with a colloidal monolayer of polystyrene (PS) microspheres was used to prepare microstructured metal oxide honeycomb films. In contrast to unstructured PSCs, the PSCs with honeycomb structures exhibit higher open-circuit voltage and fill factor, due to the strong absorption ability of the perovskite crystals within the honeycomb. Such PSCs have semi-transparent properties and a PCE of up to 9.5% with highly average visible transmission of the active layer (∼37%). In addition, the honeycomb scaffold in such a semi-transparent PSC can efficiently inhibit the electronic contact between the compact TiO_2 and the hole-conductor, resulting in a low shunt resistance [Fig. 7(b)].

2. 2D PC

Choi *et al.*[92] demonstrated that a PSC with a compact 2D PC nanodisk array electron transport layer can greatly enhance light harvesting of PSC. The nanosphere lithography technique was employed to prepare the 2D PC nanodisk array by using a monolayer of self-assembled polymer spheres as a template with varying the size of the polymer spheres.

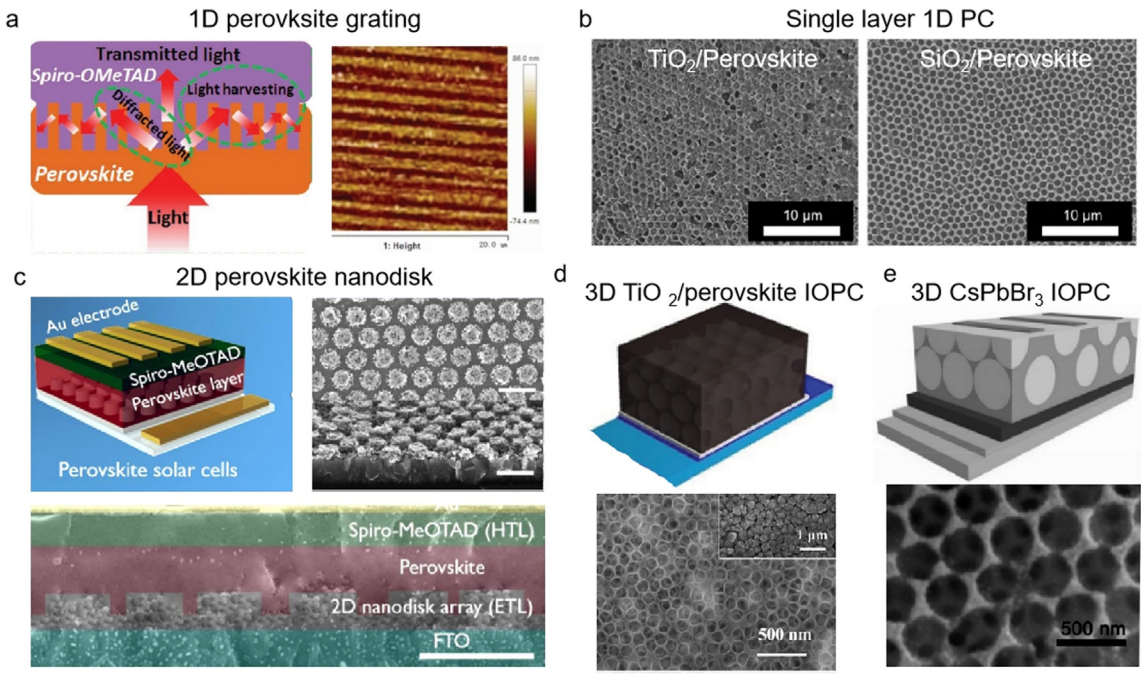

FIG. 7. Light trapping enhancement of PSCs based on PCs. (a) Schematic diagram of diffracted grating PSCs and AFM image of diffraction grating perovskite film. Adapted with permission from Wang *et al.*, Adv. Energy Mater. **8**, 1870052 (2018). Copyright 2018 Authors, licensed under a Creative Commons Attribution (CC BY) license. (b) SEM images of TiO_2/perovskite film and SiO_2/perovskite film. Reproduced with permission from Hörantner *et al.*, Energy Environ. Sci. **8**, 2041–2047 (2015). Copyright 2015 Royal Society of Chemistry.[157] (c) Schematic diagram for PSCs integrating with a 2D nanodisk array (left), top view and cross-sectional SEM images of the 2D nanodisk array (right), and SEM (cross section) image of PSC (the scale bar = 1 μm). Adapted with permission from Choi *et al.*, Nano Energy **56**, 365–372 (2019). Copyright 2019 Authors, licensed under a Creative Commons Attribution (CC BY) license. (d) Schematic diagram of TiO_2 inverse opal electron transport layer-based PSCs, and SEM image of TiO_2 inverse opal-like electron transport layer. Adapted with permission from Chen *et al.*, J. Phys. Chem. C **7**, 137 (2015). Copyright 2015 Authors, licensed under a Creative Commons Attribution (CC BY) license.[84] (e) Schematic diagram of CQD/$CsPbBr_3$ inverse opal PSCs, and SEM image of a CQD/$CsPbBr_3$ inverse opal film. Adapted with permission from Zhou *et al.*, Adv. Mater. **29**, 1703682 (2017). Copyright 2015 Authors, licensed under a Creative Commons Attribution (CC BY) license.[89]

They found that the light harvesting in the perovskite layer was significantly enhanced by integrating with nanodisk arrays, which displayed strong forward scattering and confinement effects. Meanwhile, the charge transport was also enhanced owing to reducing contact resistance between the ND array electron transport layer and the perovskite layer. The power conversion efficiency of PSCs with ND arrays as electron transport layers reached 19%, with low photocurrent-voltage hysteresis, which was ∼13% higher than that of the pristine PSC [Fig. 7(c)].

3. 3D PC

Chen *et al.*[84] replaced traditional compact layers and scaffold layers with a multifunctional inverse opal-like TiO_2 electron transport layer (IOT-ETL) in PSCs. Benefitting from the PC effect of the IOT-ETL film, the light harvesting efficiency was improved, leading to an improvement of the J_{sc} of the PSCs. Moreover, the bottom of the IOT-ETL film significantly restricted the charge recombination, which resulted in an increase in the open circuit voltage. Eventually, the PCE of the IOT-ETL-based PSC reached a value of ∼13.11%, while that of the conventional P25 mesoporous layer-based perovskite solar cells is ∼11.00% [Fig. 7(d)]. Recently, perovskite quantum-dot-based PSCs have been extensively explored, but their PCEs are still somewhat restricted, limited by the relatively weak light utilization ability of perovskite quantum dots owing to wide bandgap, resulting in a relatively low photocurrent density. Zhou *et al.*[89] used a template-assisted method to fabricate the $CsPbBr_3$ perovskite inverse opal (IO) films and further integrated with carbon quantum dots (CQD) through the spin-coating approach. $CsPbBr_3$ IO films served as supporters with tunable photonic bandgaps within the visible region, which introduced a slow-photon effect to enhance light absorption ability. CQDs attached on the IO frameworks acted as a sensitizer to broaden the light absorption range and accelerate charge transfer process. In contrast to pristine $CsPbBr_3$ PSCs, the PCE of CQD/$CsPbBr_3$ IO PSCs reached ∼8.29%, which enhanced more than two times [∼3.48% in $CsPbBr_3$ PSCs; Fig. 7(e)]. Daem *et al.* theoretically simulated the optimum pore size of a 3D inverse opal (3D-IO) photonic nanostructuration through a home-made genetic algorithm (GA) and a coupled-wave analysis (RCWA), and could experimentally demonstrated that the $MAPbI_3$-PS500 3D-IO photonic nanostructuration with 500-nm-diameter spherical pores obtained optimal light absorption.[98]

C. Colorful PSCs by using 1D-2D PCs

1. 1D colorful PSCs

After the development of past few years, the PCE of PSCs has reached more than ∼25% and is likely to make a further

breakthrough. However, the color gamut of PSCs in the built environment is very limited, which is a disadvantage in market competition with organic photovoltaics devices. In addition to the LHE enhancement, the 1D PC can be utilized to construct colorful PSCs depending on the reflective properties of the PC. For example, Zhang *et al.*[85] integrated a porous 1D PC scaffold into a PSC, which consists of alternating layers of dense TiO_2 and porous SiO_2. The photovoltaic devices presented an efficiency of 4%–9% with tunable color covering the entire visible spectrum [Figs. 8(a)–8(c)]. Ramírez Quiroz *et al.*[158] combined semitransparent PSCs with dielectric mirrors, which simultaneously offers the desired color and enhances the light harvesting of PSCs. Such colorful PSC demonstrates an improved photocurrent density with dielectric mirrors ∼21%, and high device transparency values (∼31%), as shown in Fig. 8(d). Similarly, Yoo *et al.*[159] integrated 1D PC filter of a nonperiodic SiO_2/TiO_2 multi-monolayer with PSC to develop colorful (red, green, and blue) PSCs. Compared with a control PSC with PCE of ∼20.1%, the PCEs of the PSCs with 1D PC filter show a small loss (<10%), owing to the narrow bandwidth of 1D PC filter originating from the advantages of multilayering nonperiodic high-index TiO_2/low-index SiO_2. In addition, the photostability of the PSCs with 1D PC filter was enhanced due to UV blocking by TiO_2 layers [Figs. 8(e) and 8(f)].

2. 2D colorful PSCs

Meng *et al.*[160] prepared two-dimensional inverse-opal $MAPbI_3$ films with vivid reflection colors via template removal method. The PCSs with $MAPbI_3$ films as light absorbing layers show vivid colors as well as a respectable PCE of ∼11.2%. The same group further fabricated two kinds of ETLs with 2D PC structures, including SnO_2 and an SnO_2–TiO_2 composite with the similar method. These two ETLs were shown to exhibit large-scale 2D superlattice structures and tunable structural colors with varying viewing angles. The $MAPbI_3$-based PSCs achieved an efficiency of 16.8% with structural colors when incorporated ETLs into them, owing to the excellent electron transfer ability and vivid colors [Figs. 8(g)–8(i)].[95] Similarly, Limin Qi's group[161] realized colorful PSCs when integrating TiO_2 nanobowl arrays as ETLs, which displayed angle-dependent vivid colors, and produced an efficiency of 16.94% [Figs. 8(j)–8(l)].

D. Photon recycling of PCs for PSCs

Generally, photon recycling has a significant impact on the total open-circuit voltage in PSCs.[162] The amount of light coupled out from a PSC strongly depends the structures of the cells themselves. In a planar device, only a part of the photons can emit into the escape cone that leads to emission, while most of the photons encounter total

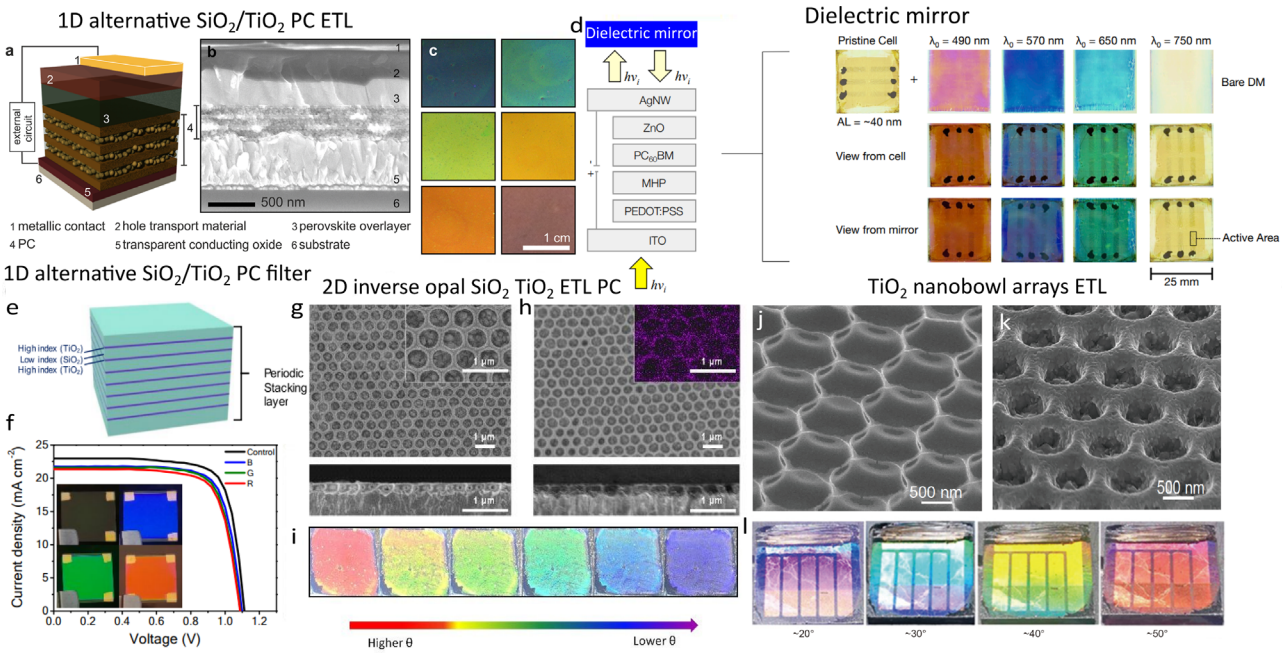

FIG. 8. Colorful PSCs based on 1D PC. (a)–(c) Schematic illustration, cross-sectional SEM image, devices colors integrating different PCs. (a)–c) Reproduced with permission from Zhang *et al.*, Nano Lett. **15**, 1698–1702 (2015). Copyright 2015 American Chemical Society.[85] (d) Devices architecture and digital images of a 1D PC-based PSC, and 1D PC consists of alternative SiO_2 and TiO_2 layers. Reproduced with permission from Ramírez Quiroz *et al.*, ACS Nano **10**, 5104–5112 (2016). Copyright 2016 American Chemical Society.[158] (e) and (f) Schematic diagram of 1D PC made from periodic stacking of alternative TiO_2 and SiO_2 layers, EQE spectra of 1D PC-based PSCs with various bandwidths at blue, green, and red, respectively. The inset presents a digital photo.[159] Reproduced with permission from Yoo *et al.*, ACS Nano 13, 10129–10139 (2019). Copyright 2019 American Chemical Society. (g) and (h) SEM images of the inverse opal structured SnO_2 and inverse opal structured SnO_2–TiO_2 composite films on FTO substrates. (i) Digital photos of the 2D PC perovskite films as a function of angle.[95] Reproduced with permission from Liu *et al.*, Nanoscale 12, 8425–8431 (2020). Copyright 2020 Authors, licensed under a Creative Commons Attribution (CC BY) license. (j) and (k) SEM images of TiO_2 and PVK@TiO_2 nanodisk array. (l) Digital photos of colorful PSCs with varying viewing angles.[161] Reproduced with permission from Wang *et al.*, Sci. China Mater. **36**, 35–46 (2020). Copyright 2020 Springer Nature.

internal reflection and are subsequently re-absorbed, and all photons are virtually desired to be emitted via optimal coupling in a device. The theoretical analysis was carried out by Nanz *et al.*,[93] where the careful wave-optical calculations are demanded to ascertain the open-circuit voltage enhancement ($\Delta V_{OC}{}^{PR}$). Considering the absorption, the probability of radiative emission, and photon recycling in a device, $\Delta V_{OC}{}^{PR}$ can be determined by the following equation:

$$\Delta V_{OC}{}^{PR} = \frac{k_B T_C}{e} \mathrm{In}\left(\frac{1}{1-(1-p_e-p_a)\gamma_{\mathrm{int}}}\right), \tag{14}$$

where p_a and p_e present the probabilities of a regenerated photon being reabsorbed and radiatively re-emitted. k_B, e, and T_C are the Boltzmann constant, the elementary charge, and the operating temperature of solar cells assuming to be T_C= 300 K. They revealed that photon recycling relies on both the optical and electronic character of the solar cells and they divided the maximum improvement of open-circuit voltage into two cases: (i) 50–100 mV for an inefficient outcoupling device (e.g., planar devices), and (ii) 10–50 mV for an efficient outcoupling device (e.g., textured devices). Meanwhile, light trapping in devices enhances the light outcoupling accompanying by decreasing the proportion of reabsorbed photons, which further improves the carrier concentration and the photovoltage of the devices. Thus, when designing the light trapping structures, photon recycling is reduced in contrast to a planar device. In contrast, the light incoupling into the cells increases as implanting the nanotextured interfaces, resulting in an increase in the short-circuit current density instead of the open-circuit voltage. Hence, it is significant to fully comprehend how the photon recycling impacts on light emission and open-circuit voltage in PSCs. Nanz *et al.*[93] integrated a nanotextured biperiodic perovskite (2D PC) thin film into PSCs with multilayer stack and quantitatively analyzed the influence of photon recycling on the open circuit voltage relying on a full-wave optical simulation, in which open-circuit voltage in PSCs can achieve an increase in 2%. Moreover, the nanopattern structure presented a bigger photon recycling rate than that of the ideal Lambertian case. Previously, the design of PSCs has been mainly focused on the optimization of light harvesting, while photon recycling is often ignored and it is important in future designs of PSCs.

E. Others: UV illumination stability and energy transfer

The instability and performance deterioration of PSCs under UV illumination still limits the practical applications. The PC structure can effectively prevent direct illumination of UV light on PSCs. Zheng and Xuan[90] employed a photon management structure including a 1D-PC stacking alternately two materials with different refractive indices and a self-cleaning biomimetic moth-eye structure for simultaneously screening the semitransparent $CH_3NH_3PbI_3$ PSCs from the harmful UV irradiation and boosting the light harvesting for visible–near-infrared (Vis-NIR) lights. With optimizing the photon management structure in PSCs, they achieved a high reflection for the UV band as well as low reflection for the Vis-NIR band. This significantly suppresses the adverse effects of UV light, thereby enhancing the performance of PSCs. Zhou *et al.*[163] fabricated a $CsPbBr_3$ IO through the template removable method, and further integrated it with crystalized Si QDs, which remarkably enhanced the solar energy utilization efficiency owing to a fluorescence resonance energy transfer process from the Si QDs to the $CsPbBr_3$ IO. Si QDs act as donor to emit photoluminescence, which can be absorbed by $CsPbBr_3$ (acceptor), bringing about an increase in the carrier population in PSCs. An enhanced power conversion efficiency up to 8.31% along with an improved photocurrent density up to 7.8 mA cm^{-2} was observed in PSCs after integrating with Si QDs.

Lead with halogen atoms, atoms of organic groups and perovskite compounds show an outstanding photovoltaic performance, for instance, t suitable forbidden band widths, wide range of spectral absorption, high carrier diffusion lengths, and so on. However, the toxicity issue and water solubility of lead hinders large-scale commercial applications, especially for PSCs.[164] Therefore, in order to develop environmentally friendly lead-free PSCs, it is necessary to explore non- or low-toxic perovskite materials. Generally, some of the less toxic metal cations, such as Bi^{3+}, Sb^{3+}, Ge^{2+}, Sn^{2+}, Cu^{2+}, and Mn^{2+}, were used to replace Pb^{2+} in perovskite to form lead-free perovskites. The lead-free perovskites based on these metal cations not only increase the diversity of species, but also change the environmental stability of the PSCs. Among these non- or low-toxic perovskite materials, Sn^{2+}-based lead-free perovskite exhibits excellent photoelectric properties. Due to the similar electronic structures and ionic radii of Sn^{2+} and Pb^{2+}, the PCE of Sn^{2+}-based PSCs can reach more than 10%.[165] It is worth noting that in practical applications, the absorbing layer of PSCs is required to be stable under illumination, humidity, air exposure, and high-temperature conditions. Unfortunately, Sn^{2+} will spontaneously oxidize to Sn^{4+} in air, which hinders the development of Sn^{2+}-based PSCs. The decomposition results in product SnI_2, which has the same toxicity as PbI_2.[166] Ge^{2+} is also considered to be a suitable alternative to Pb^{2+}. However, due to the small ionic radius of Ge^{2+} and the low solubility of the precursor in polar solvents, the Ge^{2+}-based perovskite has a relatively wide bandgap. Furthermore, the morphology is difficult to control, the performance of the PSCs is poor, and the PCE is low. In addition, Ge^{2+} will also change to the more stable ionic state Ge^{4+}, so reducing the stability of the Ge^{2+}-based PSCs.[167] Although Cu^{2+} is in a stable oxidation state, its ionic radius is small and is difficult to crystallize into an ideal perovskite structure, which leads to low intrinsic conductivity and absorption coefficient of the Cu^{2+}-based perovskite layer.[168] By this token, the development of lead-free perovskites and perovskite devices based on photonic crystals deserves more efforts.

VII. PCS FOR PDS

PDs are key components for converting optical signals into electrical signals in a variety of applications, such as optical communications, imaging, and environment monitoring. Semiconductor materials are the core component of the PDs. Up to now, multiple kinds of semiconductor materials have been explored in PDs, including Si, carbon nanotubes, and III-V compounds. However, PDs based on the above-mentioned semiconductor materials usually require expensive equipment, strict fabrication processes, and operating conditions. Perovskite materials have been recognized as a promising semiconductor for various optoelectronic devices due to their large optical absorption coefficient, long carrier diffusion length, high carrier mobility, and tunable bandgap.[32,169] More importantly, the preparation cost of low-temperature solution-processing perovskite materials is low using the simple production process. Perovskite PDs seize the opportunity to integrate with the most advanced circuits, which offer high sensitivity and ultrafast response speed. Some significant parameters

are employed to perform the performance of PDs: The spectral responsivity (R) is a representative parameter to examine the photodetecting ability of the PDs, which can be expressed as[77]

$$R = \frac{I_{ph} - I_{dark}}{PS}, \tag{15}$$

where I_{ph} presents the photocurrent, I_{dark} is the dark current, P represents the light power density, and S is the effective area under irradiation. The detectivity (D^*) reflects the capability to acquire weak signals from the noise environment, expressed as

$$D^* = \frac{R}{(2eI_{dark}/S)^{1/2}}. \tag{16}$$

Currently, perovskite PDs with a planar metal–semiconductor–metal (MSM) structure have been extensively explored because of their simplicity and integration advantages. Hu *et al.*[170] reported the first perovskite MSM PD with an ITO–perovskite–ITO structure and achieved high photoresponsivities of 3.49 and 0.0367 A/W at 365 and 780 nm, respectively. Hereafter, a lot of efforts have been devoted to further enhance the performance of PDs by perfecting light harvesting and the charge carrier diffusion length and mobility, etc., which could be improved with better morphology and higher crystalline quality of perovskite. Very recently, PCs were adopted to boost the performance of perovskite PDs through improving the light harvesting, interfacial-tunneling effect, and enhancing the quality of the perovskite films. In this section, we will review the main progress of perovskite PDs based on PCs.

A. 1D PC

Liu *et al.*[171] fabricated $CsPbBr_3$ nanonet films (NFs) grown in the preferred (110) orientation through a confined growth method of monolayer nano-PS sphere. Such a system was beneficial for facilitating charge carrier transport and enhancing light harvesting efficiency. The (110)-orientation-preferred $CsPbBr_3$ NFs-based PDs demonstrated the best performance, which displayed the largest linear dynamic range of up to 120 dB; meanwhile, the responsivity and detectivity of 2.84 AW^{-1} and 5.47×10^{12} Jones were also realized [Figs. 9(a) and 9(b)]. Wang *et al.*[86] employed

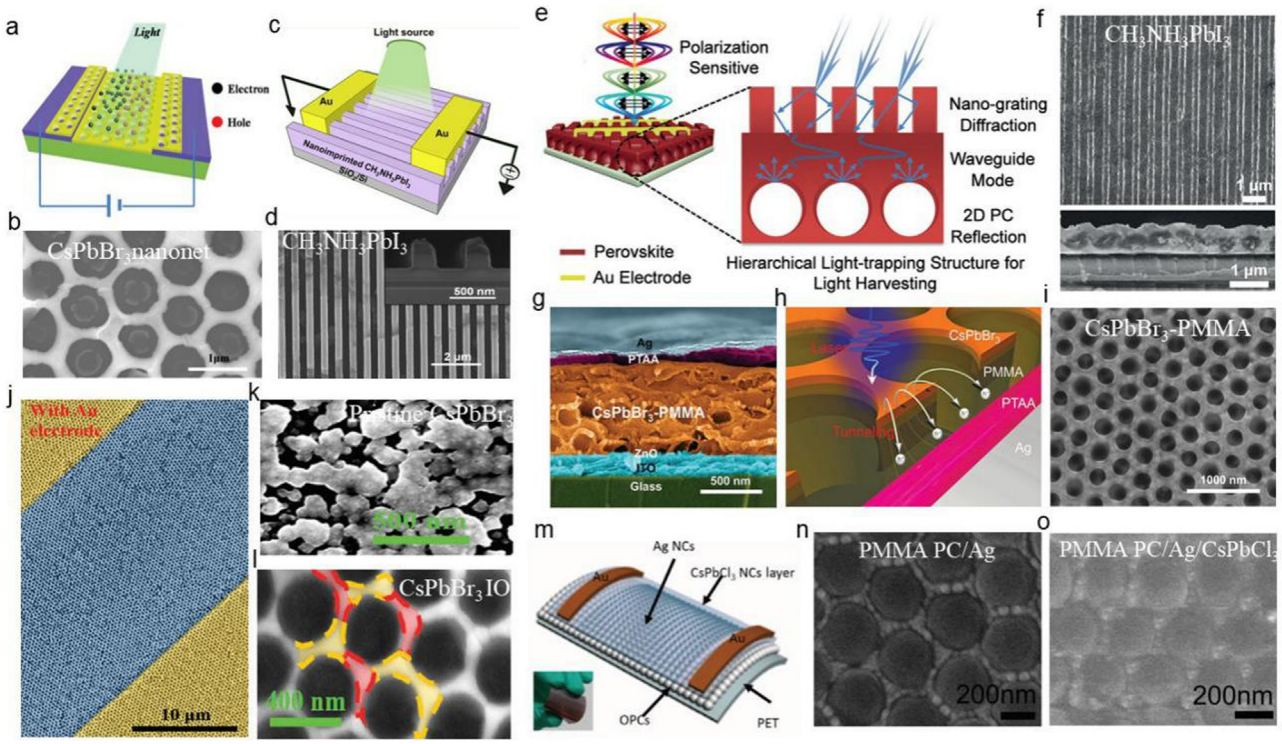

FIG. 9. PC for perovskite PDs. (a) and (b) Schematic illustration of a perovskite nanonet PD, and SEM image of $CsPbBr_3$ nanonet film. Reproduced with permission from Liu *et al.*, Nanoscale **11**, 9302–9309 (2019). Copyright 2019 Royal Society of Chemistry.[171] (c) and (d) Schematic illustration of a nanograting perovskite PD, and SEM image of a nonimprinted perovskite $CH_3NH_3PbI_3$ thin film imprinted with a Si nanograting mold. Reproduced with permission from Wang *et al.*, ACS Nano 10, 10921–10928 (2016). Copyright 2016 American Chemical Society.[86] (e) and (f) Illustration of 1D nanograting bonded porous 2D-PC perovskite PD. Reproduced with permission from Angew. Chem., Int. Ed. **131**, 16608–16614 (2019). Copyright 2019 Wiley.[172] (g) Cross-sectional SEM image of the PD device. (h) Design of charge-tunneling-layer enhanced $CsPbBr_3$-based PDs: Sketch of tunneling effect of carriers (h^+) after laser excitation. (i) SEM image of a space-confined $CsPbBr_3$ IO film.[173] Reproduced with permission from Zeng *et al.*, Adv. Funct. Mater. **29**, 1904461 (2019). Copyright 2019 Wiley. (j) SEM image of a $CsPbBr_3$ IO film with large area. (k) and (l) SEM images of conventional and space-confined $CsPbBr_3$ film.[174] Reproduced with permission from Zeng *et al.*, Adv. Funct. Mater. **28**, 1804394 (2018). Copyright 2018 Wiley. (m) Schematic of the $CsPbCl_3$ on Ag/OPCs PD. (n) and (o) SEM images of PMMA OPCs, $CsPbCl_3$/OPCs, Ag/OPCs, and $CsPbCl_3$/Ag/OPCs hybrids film. Adapted with permission from Li *et al.*, Adv. Mater. **28**, 1804429 (2018). Copyright 2018 Authors, licensed under a Creative Commons Attribution (CC BY) license.[77]

the nanoimprint lithography to obtain nanoscale-patterned perovskite PDs. Compared to the nonimprinted conventional thin-film PDs, the performance of the nanoimprinted metal–semiconductor–metal PDs was remarkably boosted, approximately 35 times improvement of responsivity. The nanograting PDs achieve a high responsivity of 24.1 and 58.5 A/W at the wavelength of 466 and 635 nm, respectively, with a bias voltage of 1 V. The performance of the nanograting PD is ∼30 times higher than that of the reference PD and more than two orders of magnitude better than the commercial Si PD. Such enhancement was attributed to a nanograting-induced better photon absorption and charge carrier transport, and higher crystallinity [Figs. 9(c) and 9(d)].

B. 2D PC

With the rapid development of information technology, perovskite PDs with high-responsivity and the ability of polarization-sensitive light detection are demanded. Zhan *et al.*[172] designed and fabricated a 1D nanograting bonded porous 2D photonic crystal perovskite photodetector (G-PC-PD) using a commercial DVD master and 2D crystalline colloidal arrays template. The coupling effect from grating diffraction and reflection of the PC stop band efficiently enhanced light harvesting of G-PC-PD. Meanwhile, the porous scaffold and nanoimprinting process offer a highly crystalline perovskite film. The G-PC-PD showed a high light responsivity and detectivity of 12.67 AW^{-1} and 6.28×10^{13} Jones and improved 6–7 times that of a pristine perovskite PD. In addition, the polarization-sensitive light detection was realized by using the ordered nanograting arrays of G-PC-PD with a rate of @0.72 $nA^{\circ -1}$. The butterfly-inspired hierarchical light-trapping structured perovskite provides a promising prospect for employing morphology engineering toward high-performance optoelectronic devices [Figs. 9(e) and 9(f)]. Chun *et al.*[91] demonstrated a vertically grown halide perovskite (VGHP) nanopillar PD through a nanoimprinting crystallization technique, employing the nanopatterned polymer stamps to form VGHP nanopillars ($CH_3NH_3PbI_3$) film. The $CH_3NH_3PbI_3$ films present low defect density (5.27×10^{17} to 9.81×10^{16} cm^{-3}) and high conductivity. Two-terminal lateral PDs based on the VGHP nanopillar films exhibited a significantly improved photoresponse.

Inorganic perovskite-based PDs usually showed high responsivity and fast response speed, while with low detectivity owing to the high dark current of the PDs. Haibo Zeng's group[173] introduced a tunneling organic layer into the PDs, in which the photogenerated charge carriers flowed across the interfacial poly(methyl methacrylate) PC layer by the called Fowler–Nordheim tunneling effect. The photo-/dark-current ratio of PD reaches a giant value of 2.13×10^8, and the detectivity is as high as 1.24×10^{13} Jones. The PD array realized the imaging week light signals of 244 pW. The hydrophobic organic layer effectively inhibited the destruction of the perovskites caused by moisture and ion migration [Figs. 9(g)–9(i)].

C. 3D PC

The poor perovskite film quality with the low solubility of precursor and uncontrollable film growth restricts their applications in PDs. Haibo Zeng's group[174] employed a space-confined growth strategy with 3D inverse opal PC to conquer the low solubility and fast crystal growth disadvantages through freezing the precursor solution within the gaps of ordered polystyrene sphere templates. $CsPbBr_3$ polycrystalline high-quality films with low trap density (3.07×10^{12} cm^{-3}) and high carrier mobility (9.27 cm^2 V^{-1} s^{-1}) were obtained. PDs based on these films exhibited a responsivity of 216 A W^{-1}, a response speed (<5 μs), and high detectivity of 7.55×10^{13} and 3.1×10^5 Hz^{-3} dB bandwidth [Figs. 9(j)–9(l)]. Our group combined surface plasmon and photonic crystal effects (3D PMMA PC), in which the luminescent intensity of $CsPbCl_3$ NCs in $CsPbCl_3$/Ag/OPCs hybrids was enhanced more than 150-fold. The high-performance flexible UV PD was fabricated using these hybrids, exhibiting a high detectivity of 9×10^{14} Jones and narrow response linewidth of 30 nm, much better than the commercial silicon PDs. The photocurrent enhances 682%, and the response time reduces 42.5% and 40.4% in $CsPbCl_3$/Ag/OPCs flexible film [Figs. 9(m)–9(o)].[77] Heeyoon *et al.* utilized a transfer-printed PS microbead monolayer on perovskite/PMMA to enhance the mechanical durability, environmental stability, and optical properties of the perovskite PDs. The optimal D^* of PMMA/PS PDs is 16.1×10^{10} Jones for 700 nm light.[96] Our group obtained double narrowband flexible NIR PDs based on PMMA/$NaYF_4$:Yb^{3+}, Er^{3+}@$NaYF_4$:Nd^{3+}/$MAPbI_3$ hybrids, which have the photoresponse to the 808 and 980 nm light with 3.01×10^{11} Jones and 2.68×10^{11} Jones of D^*, respectively.[175] We divided the perovskite photonic crystal devices into four categories, including PSCs, LED, laser, and PDs. Related performance parameters are summarized in Table I.

VIII. SUMMARY AND OUTLOOK

A rapid progress in the research on PC (1D, 2D, and 3D)-based perovskite photonic/photoelectric devices has recently been witnessed. A timely and concise summary on the earlier and current achievements is therefore called for in order to assist the further progress of a formulated development of this very promising research field. In this article, we divided the perovskite photonic crystal devices into four categories as shown in Schematic 3. We reviewed perovskite PCs from both theoretical and experimental points of view. Among other aspects, we recapitulated the improvement of PCs concerning light absorption and spontaneous emission using perovskite materials, the enhanced light-emission/extraction efficiency of LEDs, and the reduction of the pumping threshold of perovskite lasers. We attended the fact that PC-generated enhancement of the light harvesting of perovskite materials has been employed to construct highly sensitive PDs and colorful and efficient PSCs. Such improvements are attributed to photonic bandgap and slow photon effects, photon recycling, and/or structural effects.

In future studies, we believe that the following several points should be taken into account and emphasized. First of all, PCs divide into opal and inverse opal, as well as 1D, 2D, and 3D classes, with advantages and disadvantages. Because of different pore sizes and volume-surface ratios, 2D and 3D inverse opal PCs are more suitable for PSCs than 1D PCs. However, 1D PCs process the superiority of faster charge transport, lower exciton recombination rates, and higher transparency, which may be more suitable for PDs. On the other hand, compared with the 1D and 3D PCs, 2D PCs or arrays have the advantages of high controllability that the light-induced electrons can

TABLE I. Summary of device performance of perovskite photonic crystal devices.

PCs for PSCs	PCs	Methods	J_{sc} (mA/cm^2)	V_{OC} (V)	FF (%)	η A(%)	With or without PC	Reference
Light trapping enhancement	1D perovskite grating	CD/DVD imprinted	21.67	1.078	71.52	16.71	W.O.	156
			23.11	1.1111	76.75	19.71	Grating	
	Monolayer TiO_2-SiO_2 1D PC	Monolayer lithography	10.1	0.76	52	4.0	Pristine	157
			17.1	0.84	66	9.5	1D PC	
	Hemisphere TiO_2 PC	Nano-imprint technique	18.0	0.93	62.8	10.5	Pristine	155
			26.5	0.92	62.4	15.2	PC	
	2D perovskite nanodisk array	Template etching	20.58	1.06	0.69	15.51	Pristine	92
			22.73	1.11	0.71	18.70	Nanodisk	
	3D IOPC TiO_2 ETL	Template removal method	19.90	···	···	11.00	Pristine	84
			23.93	0.972.8	61	13.11	3D IOPC	
	CQD/$CsPbBr_3$ IO	Template removal method	7.46	0.82	0.57	3.48	Pristine	89
			9.25	0.93	0.61	5.25	$CsPbBr_3$ IOPC	
			11.34	1.06	0.69	8.29	CQD/$CsPbBr_3$ IO	
Colorful PSCs	SiO_2/TiO_2 1D PC (Inside the PSC)	Alternated deposition	13.44	0.98	0.67	8.8	Blue	85
			10.4	0.95	0.71	7.0	Blue-green	
			9.9	0.92	0.74	6.7	Green	
			9.9	0.95	0.71	6.6	Orange	
			7.6	0.93	0.62	4.5	Red	
	SiO_2/TiO_2 multi Nanolayer filter 1D PC (Outside the PSC)	Depositing alternatively high- and low-index materials	23.0	1.15	76	20.1	Control	159
			20.9	1.12	77	18	Red	
			21.3	1.13	77	18.6	Green	
			21.4	1.13	78	19.4	Blue	
	Dielectric mirrors	···	5.40	1.03	65.6	3.6	Pristine	158
			6.06	1.03	65.6	4.1	$\lambda = 490$ nm	
			5.96	1.03	65.6	4.0	$\lambda = 570$ nm	
			6.33	1.03	65.6	4.3	$\lambda = 650$ nm	
			6.23	1.03	65.6	4.2	$\lambda = 750$ nm	
	2D inverse opal SnO_2-TiO_2 ETL PC	Template removal method	20.2	0.98	51	10.2	SnO_2 ETL PC	95
			20.3	1.09	75	16.8	SnO_2-TiO_2 ETL PC	
	TiO_2 nanobowl arrays ETL	Interfacial lithography	2.59	1.04	72.0	16.94	TiO_2 nanobowl	161
Photon recycling for PSCs	···	···	18.1	0.02	···	···	W.O.	93

PCs for perovskite Lasers	PCs	Methods	Lasing threshold W/cm^2	Energy density threshold μJ/cm^2	Linewidth nm	With or without PC	Reference
1D PCs	Distributed feedback cavity	Thermal nanoimprint lithography process	13	···	0.7	Grating	133
On top of 2D PCs	Si PC slabs	Nanoimprint lithography, Si thin-film deposition, and crystallization techniques	···	···	~40	2D PCs	134
	PMMA PCs	Template fabrication	···	68.5 ± 3.0	0.24	2D PCs	87
2D PCs	$MAPbI_3$ thermal imprint	Thermal nanoimprint	···	3.8	0.13	2D PCs	135
Inserted in 3D PCs	Poly(St-MMA-AA)	Self-assembly method	···	35.5	4.6	3D PCs	136
	Conjugated polymer particles	Self-assembly method	···	1.3×10^4	<0.5	3D PCs	137
3D PCs	PS	Templating approach	···	1.6×10^4	0.15	3D IO PCs	138

TABLE I. (*Continued.*)

PCs for perovskite Lasers	PCs	Methods	Lasing threshold W/cm^2	Energy density threshold μJ/cm^2	Linewidth nm	With or without PC	Reference
CLCs	Glass/CLC/Al_2O_3/ $MAPbI_3$/PMMA/Au	···	···	50	···	1D PCs	82
	All-inorganic perovskite QDs doped CLCs	···	···	0.15	0.2	1D PCs	140

PCs for perovskite LEDs	PCs	Methods	EQE (%)	PLQY (%)	With or without PC	Reference
Perovskite nanophotonic substrates	TiO_2	Two-step anodization	17.5	35	Anodic alumina membranes	94

PCs for PDs	PCs	Methods	Response Wavelength nm	R A/W	D^* Jones	With or without PC	Reference
1D PC	PS	···	473	2.84	5.47×10^{12}	1D PC	149
	Perovskite nano-grating	Nanoimprint	466	24.1	···	Grating	86
			635	58.5	···		
2D PC	1D nano-grating bonded porous 2D PC	DVD/2D crystalline colloidal arrays template	White light	12.67	6.28×10^{13}	1D and 2D PC	171
	Two-terminal lateral PDs	Vertically grown	520	1	5×10^{9}	1D nanoarrays	91
	ITO/ZnO/$CsPbBr_3$-PMMA/PTAA	Template removal method	442	0.34	1.24×10^{13}	IO PC	173
3D PC	$CsPbBr_3$ IO film	Template removal method	442	216	7.55×10^{13}	3D PC	174
	$CsPbCl_3$/Ag/OPCs hybrids	Self-assembly method	365	8.1	9×10^{14}	3D PMMA PC	77
	PMMA/PS bead	Unidirectional rubbing and assembled method	465	3.49×10^{-2}	1.33×10^{11}	3D PC	96
			500	4.23×10^{-2}	1.61×10^{11}		
			610	2.38×10^{-2}	8.76×10^{10}		
			700	1.9×10^{-2}	7.22×10^{10}		
	PMMA/$NaYF_4$:Yb^{3+}, Er^{3+}@$NaYF_4$:Nd^{3+}/ $MAPbI_3$ hybrids	Self-assembly method	808	8.1	3.01×10^{11}	3D PMMA PC	175
			980	8.1	2.68×10^{11}		

be transferred along the tube wall and of a decreased exciton recombination at the intergranular interface. Therefore, a proper choice of PCs is essential for a good device performance. Second, it still remains a great challenge to apply conventional patterning techniques to construct compact, dense, and functional PC structures for devices. The present fabrication techniques for PCs, such as self-assembling, usually induce inevitable stacking faults and disorders, which lead to poor PC bandgaps with broad and low reflection, and moderate band edges. It reduces the PC ability to enhance luminescence and localize the light efficiently. In addition, it is difficult to satisfy the thickness requirements for perovskite photoelectric devices, especially for PSCs, due to the limitations in the preparation technologies of the PCs. Currently, the photoelectric conversion efficiency of PC-based PSCs is still lagging. Therefore, the development of new strategies for fabricating large-area and high-quality thin PCs and exploring new functionalities of PCs will probably become a future development direction of PC-based devices. Third, combing PCs and other light management strategies (e.g., plasmonic enhancement, use of organic antennas) into devices at the same time could be a promising way to further improve the performance of devices. Fourthly, for practical applications, the stability of PCs (e.g., thermal, mechanical, and light stability) should be paid more attention. Thus, the scope is very wide and versatile for future research of PCs in perovskite photonic/photoelectric devices, bringing broad ramifications for technology as well as for the fundamental understanding of these promising systems.

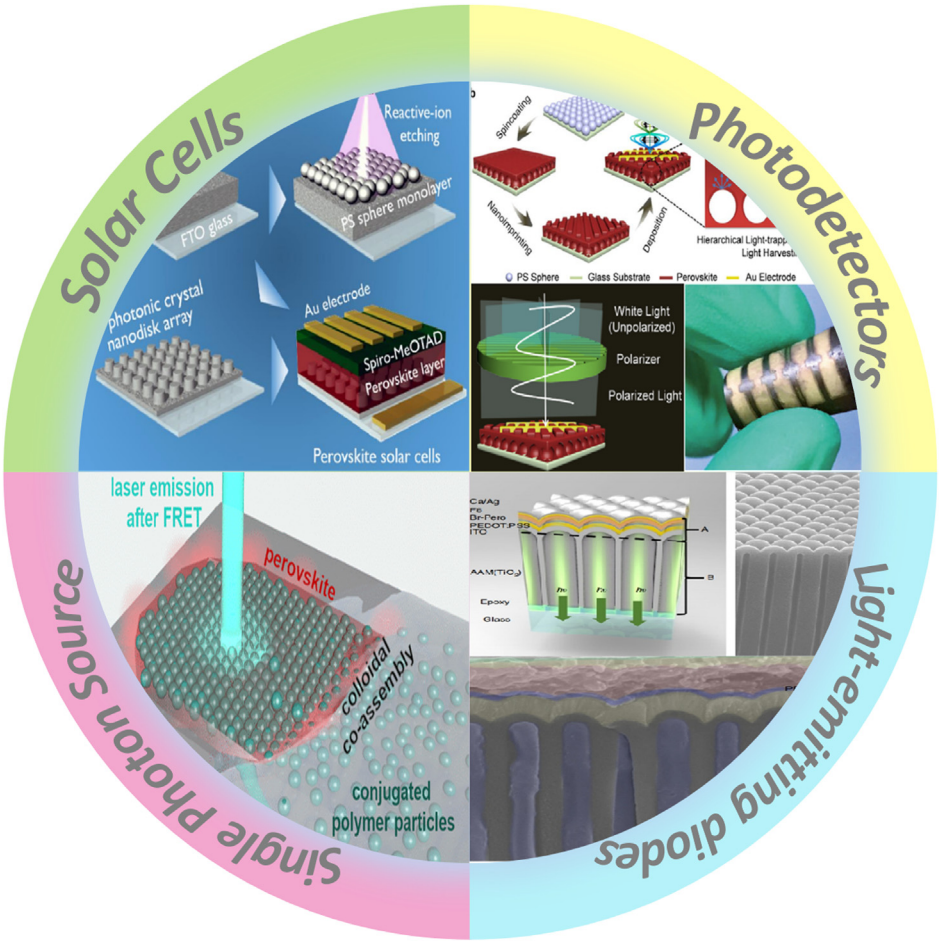

SCHEME 3. The categories of perovskite photoelectric crystal devices. The solar cells.[92] Reproduced with permission from Choi *et al.*, Nano Energy **56**, 365–372 (2019). Copyright 2019 Authors, licensed under a Creative Commons Attribution (CC BY) license. The single-photon source.[137] Reproduced with permission from Mikosch *et al.*, Chem. Mater. **31**, 2590–2596 (2019). Copyright 2019 American Chemical Society. The light-emitting diodes.[94] Reproduced with permission from Zhang *et al.*, Nat. Commun. **10**, 727 (2019). Copyright 2019 Authors, licensed under a Creative Commons Attribution (CC BY) license. The photodetectors.[172,175] Reproduced with permission from Zhan *et al.*, Angew. Chem., Int. Ed. **131**, 16608–16614 (2019). Copyright 2019 Wiley.

ACKNOWLEDGMENTS

This work was supported by the National Natural Science Foundation of China (Grant Nos. 11974143, 62175025, 12104084, and 62222502), the Outstanding Young Scientific and Technological Talents of Dalian (No. 2021RJ07), and the Natural Science Foundation of Liaoning Province (No. 2021-BS-080).

AUTHOR DECLARATIONS

Conflict of Interest

The authors have no conflicts to disclose.

Author Contributions

Yanan Ji: Conceptualization (equal); Investigation (lead); Writing – original draft (lead). **Hongwei Song:** Conceptualization (equal); Supervision (equal); Writing – review & editing (equal). **Wen Xu:** Conceptualization (equal); Writing – original draft (equal); Writing – review & editing (equal). **Ilia L. Rasskazov:** Conceptualization (supporting); Writing – review & editing (supporting). **Haichun Liu:** Writing – review & editing (supporting). **Junhua Hu:** Investigation (supporting). **Mao Liu:** Investigation (supporting). **Donglei Zhou:** Investigation (supporting). **Xue Bai:** Investigation (supporting). **Hans Ågren:** Writing – review & editing (supporting).

DATA AVAILABILITY

The data that support the findings of this study are available within the article and its supplementary material.

NOMENCLATURE

A	Absorbance
AAM/TiO_2	Anodic alumina membranes/titanium dioxide

CLCs	Chiral nematic liquid crystals
CQD	Carbon quantum dots
D^*	Detectivity
DBRs	Distributed Bragg reflectors
EQE	External quantum efficiency
EFs	Enhancement factors
EBL	Electron beam lithography
FDTD	Finite-difference time-domain
G-PC-PD	2D photonic crystal perovskite photodetector
IO	Inverse opal
IOT-ETL	Inverse opal-like electron transport layer
IPCE	Incident power conversion efficiency
LEDs	Light-emitting diodes
LHE	Light harvesting efficiency
MPP	Monodisperse poly(fluorene-co-divinylbenzene) particles
MSM	Metal–semiconductor–metal
NCs	Nanocrystals
NFs	Nanonet films
NIL	Nanoimprint lithography
NPs	Nanoparticles
OLEDs	Organic LEDs
PBGs	Photonic bandgaps
PCE	Power conversion efficiency
PCs	Photonic crystals
PSCs	Perovskite solar cells
PDs	Photodetectors
PL	Photoluminescence
PLQE	Photoluminescence quantum efficiency
PLQY	Photoluminescence quantum yield
PR	Photon recycling
PS	Polystyrene
PMMA	Polymethyl methacrylate
QDs	Quantum dots
RIE	Reactive ion etching
R	Reflection
R	Responsivity
SCs	Solar cells
SEM	Scanning electron microscope
SWG	Subwavelength grating
T	Transmission
UV	Ultra violet
VGHP	Vertically grown halide perovskite
Vis-NIR	Visible–near-infrared
1D	One-dimensional
2D	Two-dimensional
3D	Three-dimensional

Symbol

AFs	Fluorescence enhancement or reduction
AF_{exc}	Excitation altered factors
AF_{em}	Emission altered factors
$\mathbf{b}_j$	Basis vectors
c	Propagation speed of light in vacuum
D^*	Detectivity
e	Elementary charge
$\hat{\mathbf{e}}_i$	Basis vectors
$\mathbf{E}(\mathbf{r})$	Electric component
E_{PC}	Electric field intensity with the photonic crystal
E_0	Electric field intensity without the photonic crystal
$F(\lambda)$	Incident photon flux
$\mathbf{H}_{n,\mathbf{k}}$	nth Bloch mode eigenfunctions
I_{exc}	Incident excitation optical field intensity
I_{dark}	Dark current
I_{ph}	Photocurrent
J_{SC}	Short circuit current density
$\mathbf{k}$	Bloch vector
k_B	Boltzmann constant
LHE	Light harvesting efficiency
LHE_{PC}	Light harvesting efficiency with photonic crystal
LHE_0	Light harvesting efficiency without photonic crystal
$M_T(E_{21})$	Transition matrix element
n	Refractive index
P	Light power density
p_a	The probabilities of a regenerated photon being reabsorbed re-emitted
p_e	The probabilities of a regenerated photon being radiatively re-emitted
$p_0(\nu_{21})$	Photonic density of states
$p_r(E_{21})$	Electronic density of states
S	Effective irradiation area
T_C	Operating temperature
γ_{rad}	Radiative rates
γ_{tot}	Total spontaneous emission rate
γ_{guid}	Light emission rate in the form of guided mode
γ_{vert}	Light emission rate in the form of vertical mode
γ_{nrad}	Nonradiative rates
$\Delta V_{OC}{}^{PR}$	Open-circuit voltage enhancement
ΔJ_{SC}	Short-circuit photocurrent density increment
δ_{ij}	Kronecker delta
$\varepsilon(\mathbf{r})$	Dielectric constant
η_{ext}	Extracted efficiency of emission light
$\eta_{ext;0}$	Extraction efficiency of perovskite materials without the photonic crystal
η_{int}	Photo-luminescent internal quantum efficiency
η_{esc}	Photon escape probabilities
$\eta_{int;PC}$	Extraction efficiency of perovskite materials with the photonic crystal
η_{ext}	External photoluminescence quantum efficiency
$\eta_{int;0}$	Internal quantum efficiency of perovskite materials without the photonic crystal
$\eta_{int;PC}$	Internal quantum efficiency of perovskite materials with the photonic crystal
$\eta_{inj}(\lambda)$	Quantum yield of charge injection efficiency by the photo-anode
$\eta_{col}(\lambda)$	Quantum yield of charge collecting efficiency by the photo-anode
ω	Frequency

REFERENCES

[1]Q. A. Akkerman, G. Rainò, M. V. Kovalenko, and L. Manna, "Genesis, challenges and opportunities for colloidal lead halide perovskite nanocrystals," Nat. Mater. **17**, 394 (2018).

[2]J. De Roo, M. Ibáñez, P. Geiregat, G. Nedelcu, W. Walravens, J. Maes, J. C. Martins, I. Van Driessche, M. V. Kovalenko, and Z. Hens, "Highly dynamic ligand binding and light absorption coefficient of cesium lead bromide perovskite nanocrystals," ACS Nano **10**, 2071–2081 (2016).
[3]M. R. Filip, G. E. Eperon, H. J. Snaith, and F. Giustino, "Steric engineering of metal-halide perovskites with tunable optical bandgaps," Nat. Commun. **5**, 5757 (2014).
[4]Y. Fu, H. Zhu, J. Chen, M. P. Hautzinger, X. Y. Zhu, and S. Jin, "Metal halide perovskite nanostructures for optoelectronic applications and the study of physical properties," Nat. Rev. Mater. **4**, 169–188 (2019).
[5]M. V. Kovalenko, L. Protesescu, and M. I. Bodnarchuk, "Properties and potential optoelectronic applications of lead halide perovskite nanocrystals," Science **358**, 745–750 (2017).
[6]F. Liu, Y. Zhang, C. Ding, S. Kobayashi, T. Izuishi, N. Nakazawa, T. Toyoda, T. Ohta, S. Hayase, T. Minemoto, K. Yoshino, S. Dai, and Q. Shen, "Highly luminescent phase-stable $CsPbI_3$ perovskite quantum dots achieving near 100% absolute photoluminescence quantum yield," ACS Nano **11**, 10373–10383 (2017).
[7]M. Abdi-Jalebi, Z. Andaji-Garmaroudi, S. Cacovich, C. Stavrakas, B. Philippe, J. M. Richter, M. Alsari, E. P. Booker, E. M. Hutter, A. J. Pearson *et al.*, "Maximizing and stabilizing luminescence from halide perovskites with potassium passivation," Nature **555**, 497–501 (2018).
[8]A. Swarnkar, R. Chulliyil, V. K. Ravi, M. Irfanullah, A. Chowdhury, and A. Nag, "Colloidal $CsPbBr_3$ perovskite nanocrystals: Luminescence beyond traditional quantum dots," Angew. Chem. **127**, 15644–15648 (2015).
[9]L. Lang, J. H. Yang, H. R. Liu, H. J. Xiang, and X. G. Gong, "First-principles study on the electronic and optical properties of cubic ABX_3 halide perovskites," Phys. Lett. A **378**, 290–293 (2014).
[10]Q. Y. Chen, Y. Huang, P. R. Huang, T. Ma, C. Cao, and Y. He, "Electronegativity explanation on the efficiency-enhancing mechanism of the hybrid inorganic–organic perovskite ABX_3 from first-principles study," Chin. Phys. B **25**, 027104 (2015).
[11]C. Liu, W. Li, C. Zhang, Y. Ma, J. Fan, and Y. Mai, "All-inorganic $CsPbI_2Br$ perovskite solar cells with high efficiency exceeding 13%," J. Am. Chem. Soc. **140**, 3825–3828 (2018).
[12]H. Zhou, Q. Chen, G. Li, S. Luo, T. b Song, H. S. Duan, Z. Hong, J. You, Y. Liu, and Y. Yang, "Interface engineering of highly efficient perovskite solar cells," Science **345**, 542–546 (2014).
[13]A. Swarnkar, A. R. Marshall, E. M. Sanehira, B. D. Chernomordik, D. T. Moore, J. A. Christians, T. Chakrabarti, and J. M. Luther, "Quantum dot–induced phase stabilization of α-$CsPbI_3$ perovskite for high-efficiency photovoltaics," Science **354**, 92–95 (2016).
[14]W. Zhang, G. E. Eperon, and H. J. Snaith, "Metal halide perovskites for energy applications," Nat. Energy **1**, 16048 (2016).
[15]M. A. Green, A. Ho-Baillie, and H. J. Snaith, "The emergence of perovskite solar cells," Nat. Photonics **8**, 506–514 (2014).
[16]J. P. Correa-Baena, M. Saliba, T. Buonassisi, M. Grätzel, A. Abate, W. Tress, and A. Hagfeldt, "Promises and challenges of perovskite solar cells," Science **358**, 739–744 (2017).
[17]Z. Song, W. Xu, Y. Wu, S. Liu, W. Bi, X. Chen, and H. Song, "Incorporating of lanthanides ions into perovskite film for efficient and stable perovskite solar cells," Small **16**, 2001770 (2020).
[18]X. Chen, W. Xu, N. Ding, Y. Ji, G. Pan, J. Zhu, D. Zhou, Y. Wu, C. Chen, and H. Song, "Dual interfacial modification engineering with 2D MXene quantum dots and copper sulphide nanocrystals enabled high-performance perovskite solar cells," Adv. Funct. Mater. **30**, 2003295 (2020).
[19]H. H. Fang, F. Wang, S. Adjokatse, N. Zhao, J. Even, and M. Antonietta Loi, "Photoexcitation dynamics in solution-processed formamidinium lead iodide perovskite thin films for solar cell applications," Light **5**, e16056 (2016).
[20]Y. C. Zhao, W. K. Zhou, X. Zhou, K. H. Liu, D. P. Yu, and Q. Zhao, "Quantification of light-enhanced ionic transport in lead iodide perovskite thin films and its solar cell applications," Light **6**, e16243 (2017).
[21]T. Chiba, Y. Hayashi, H. Ebe, K. Hoshi, J. Sato, S. Sato, Y. J. Pu, S. Ohisa, and J. Kido, "Anion-exchange red perovskite quantum dots with ammonium iodine salts for highly efficient light-emitting devices," Nat. Photonics **12**, 681–687 (2018).
[22]Y. H. Kim, H. Cho, and T. W. Lee, "Metal halide perovskite light emitters," Proc. Nat. Acad. Sci. **113**, 11694–11702 (2016).
[23]K. Lin, J. Xing, L. N. Quan, F. P. G. de Arquer, X. Gong, J. Lu, L. Xie, W. Zhao, D. Zhang, C. Yan, W. Li, X. Liu, Y. Lu, J. Kirman, E. H. Sargent, Q. Xiong, and Z. Wei, "Perovskite light-emitting diodes with external quantum efficiency exceeding 20 percent," Nature **562**, 245–248 (2018).
[24]G. Nedelcu, L. Protesescu, S. Yakunin, M. I. Bodnarchuk, M. J. Grotevent, and M. V. Kovalenko, "Fast anion-exchange in highly luminescent nanocrystals of cesium lead halide perovskites ($CsPbX_3$, X = Cl, Br, I)," Nano Lett. **15**, 5635–5640 (2015).
[25]L. Protesescu, S. Yakunin, M. I. Bodnarchuk, F. Krieg, R. Caputo, C. H. Hendon, R. X. Yang, A. Walsh, and M. V. Kovalenko, "Nanocrystals of cesium lead halide perovskites ($CsPbX_3$, X = Cl, Br, and I): novel optoelectronic materials showing bright emission with wide color gamut," Nano Lett. **15**, 3692–3696 (2015).
[26]S. D. Stranks and H. J. Snaith, "Metal-halide perovskites for photovoltaic and light-emitting devices," Nat. Nanotechnol. **10**, 391–402 (2015).
[27]L. Zhao, K. M. Lee, K. Roh, S. U. Z. Khan, and B. P. Rand, "Improved outcoupling efficiency and stability of perovskite light-emitting diodes using thin emitting layers," Adv. Mater. **31**, 1805836 (2019).
[28]W. Zou, R. Li, S. Zhang, Y. Liu, N. Wang, Y. Cao, Y. Miao, M. Xu, Q. Guo, D. Di, L. Zhang, C. Yi, F. Gao, R. H. Friend, J. Wang, and W. Huang, "Minimising efficiency roll-off in high-brightness perovskite light-emitting diodes," Nat. Commun. **9**, 608 (2018).
[29]C. H. Kang, I. Dursun, G. Liu, L. Sinatra, X. Sun, M. Kong, J. Pan, P. Maity, E. N. Ooi, T. K. Ng, O. F. Mohammed, O. M. Bakr, and B. S. Ooi, "High-speed colour-converting photodetector with all-inorganic $CsPbBr_3$ perovskite nanocrystals for ultraviolet light communication," Light **8**, 94 (2019).
[30]L. Dou, Y. M. Yang, J. You, Z. Hong, W. H. Chang, G. Li, and Y. Yang, "Solution-processed hybrid perovskite photodetectors with high detectivity," Nat. Commun. **5**, 5404 (2014).
[31]S. F. Leung, K. T. Ho, P. K. Kung, V. K. Hsiao, H. N. Alshareef, Z. L. Wang, and J. H. He, "A self-powered and flexible organometallic halide perovskite photodetector with very high detectivity," Adv. Mater. **30**, 1704611 (2018).
[32]H. Wang and D. H. Kim, "Perovskite-based photodetectors: Materials and devices," Chem. Soc. Rev. **46**, 5204–5236 (2017).
[33]L. Gu and Z. Fan, "Perovskite/organic-semiconductor heterojunctions for ultrasensitive photodetection," Light **6**, e17090 (2017).
[34]Y. Ji, W. Xu, N. Ding, H. Yang, H. Song, Q. Liu, H. Ågren, J. Widengren, and H. Liu, "Huge upconversion luminescence enhancement by a cascade optical field modulation strategy facilitating selective multispectral narrow-band near-infrared photodetection," Light **9**, 184 (2020).
[35]C. Xie, P. You, Z. Liu, L. Li, and F. Yan, "Ultrasensitive broadband phototransistors based on perovskite/organic-semiconductor vertical heterojunctions," Light **6**, e17023 (2017).
[36]H. Dong, C. Zhang, X. Liu, J. Yao, and Y. S. Zhao, "Materials chemistry and engineering in metal halide perovskite lasers," Chem. Soc. Rev. **49**, 951–982 (2020).
[37]M. Saliba, S. M. Wood, J. B. Patel, P. K. Nayak, J. Huang, J. A. Alexander-Webber, B. Wenger, S. D. Stranks, M. T. Hörantner, J. T. W. Wang et al., "Structured organic–inorganic perovskite toward a distributed feedback laser," Adv. Mater. **28**, 923–929 (2016).
[38]H. Duim, H. H. Fang, S. Adjokatse, G. H. ten Brink, M. A. L. Marques, B. J. Kooi, G. R. Blake, S. Botti, and M. A. Loi, "Mechanism of surface passivation of methylammonium lead tribromide single crystals by benzylamine," Appl. Phys. Rev. **6**(3), 031401 (2019).
[39]H. Zhu, Y. Fu, F. Meng, X. Wu, Z. Gong, Q. Ding, M. V. Gustafsson, M. T. Trinh, S. Jin, and X. Y. Zhu, "Lead halide perovskite nanowire lasers with low lasing thresholds and high quality factors," Nat. Mater. **14**, 636–642 (2015).
[40]Y. Wang, X. Li, J. Song, L. Xiao, H. Zeng, and H. Sun, "All-inorganic colloidal perovskite quantum dots: A new class of lasing materials with favorable characteristics," Adv. Mater. **27**, 7101–7108 (2015).
[41]S. Yakunin, L. Protesescu, F. Krieg, M. I. Bodnarchuk, G. Nedelcu, M. Humer, G. De Luca, M. Fiebig, W. Heiss, and M. V. Kovalenko, "Low-threshold amplified spontaneous emission and lasing from colloidal nanocrystals of caesium lead halide perovskites," Nat. Commun. **6**, 8056 (2015).

[42]E. Tiguntseva, K. Koshelev, A. Furasova, P. Tonkaev, V. Mikhailovskii, E. V. Ushakova, D. G. Baranov, T. Shegai, A. A. Zakhidov, Y. Kivshar, and S. V. Makarov, "Room-temperature lasing from Mie-resonant nonplasmonic nanoparticles," ACS Nano **14**, 8149–8156 (2020).
[43]D. Weber, "$CH_3NH_3PbX_3$, ein Pb (II)-system mit kubischer perowskitstruktur/$CH_3NH_3PbX_3$, a Pb (II)-system with cubic perovskite structure," Z. Naturforsch. B **33**, 1443–1445 (1978).
[44]A. Kojima, K. Teshima, Y. Shirai, and T. Miyasaka, "Organometal halide perovskites as visible-light sensitizers for photovoltaic cells," J. Am. Chem. Soc. **131**, 6050–6051 (2009).
[45]G. Pan, X. Bai, D. Yang, X. Chen, P. Jing, S. Qu, L. Zhang, D. Zhou, J. Zhu, W. Xu *et al.*, "Doping lanthanide into perovskite nanocrystals: Highly improved and expanded optical properties," Nano Lett. **17**, 8005–8011 (2017).
[46]D. Zhou, D. Liu, G. Pan, X. Chen, D. Li, W. Xu, X. Bai, and H. Song, "Cerium and ytterbium codoped halide perovskite quantum dots: A novel and efficient downconverter for improving the performance of silicon solar cells," Adv. Mater. **29**, 1704149 (2017).
[47]D. Zhou, R. Sun, W. Xu, N. Ding, D. Li, X. Chen, G. Pan, X. Bai, and H. Song, "Impact of host composition, codoping, or tridoping on quantum-cutting emission of ytterbium in halide perovskite quantum dots and solar cell applications," Nano Lett. **19**, 6904–6913 (2019).
[48]N. Ding, W. Xu, D. Zhou, Y. Ji, Y. Wang, R. Sun, X. Bai, J. Zhou, and H. Song, "Extremely efficient quantum-cutting Cr^{3+}, Ce^{3+}, Yb^{3+} tridoped perovskite quantum dots for highly enhancing the ultraviolet response of Silicon photodetectors with external quantum efficiency exceeding 70%," Nano Energy **78**, 105278 (2020).
[49]C. K. Møller, "Crystal structure and photoconductivity of caesium plumbohalides," Nature **182**, 1436–1436 (1958).
[50]N. Mondal, A. De, and A. Samanta, "Achieving near-unity photoluminescence efficiency for blue-violet-emitting perovskite nanocrystals," ACS Energy Lett. **4**, 32–39 (2018).
[51]Z. J. Yong, S. Q. Guo, J. P. Ma, J. Y. Zhang, Z. Y. Li, Y. M. Chen, B. B. Zhang, Y. Zhou, J. Shu, J. L. Gu *et al.*, "Doping-enhanced short-range order of perovskite nanocrystals for near-unity violet luminescence quantum yield," J. Am. Chem. Soc. **140**, 9942–9951 (2018).
[52]S. W. Eaton, M. Lai, N. A. Gibson, A. B. Wong, L. Dou, J. Ma, L. W. Wang, S. R. Leone, and P. Yang, "Lasing in robust cesium lead halide perovskite nanowires," Proc. Natl. Acad. Sci. U. S. A. **113**, 1993–1998 (2016).
[53]M. Shoaib, X. Zhang, X. Wang, H. Zhou, T. Xu, X. Wang, X. Hu, H. Liu, X. Fan, W. Zheng *et al.*, "Directional growth of ultralong $CsPbBr_3$ perovskite nanowires for high-performance photodetectors," J. Am. Chem. Soc. **139**, 15592–15595 (2017).
[54]S. Sun, C. Zhang, K. Wang, S. Wang, S. Xiao, and Q. Song, "Lead halide perovskite nanoribbon based uniform nanolaser array on plasmonic grating," ACS Photonics **4**, 649–656 (2017).
[55]S. Aharon and L. Etgar, "Two dimensional organometal halide perovskite nanorods with tunable optical properties," Nano Lett. **16**, 3230–3235 (2016).
[56]Z. Zheng, X. Wang, Y. Shen, Z. Luo, L. Li, L. Gan, Y. Ma, H. Li, A. Pan, and T. Zhai, "Space-Confined Synthesis of 2D All-Inorganic CsPbI3 Perovskite Nanosheets for Multiphoton-Pumped Lasing," Adv. Opt. Mater. **6**, 1800879 (2018).
[57]D. Liang, Y. Peng, Y. Fu, M. J. Shearer, J. Zhang, J. Zhai, Y. Zhang, R. J. Hamers, T. L. Andrew, and S. Jin, "Color-pure violet-light-emitting diodes based on layered lead halide perovskite nanoplates," ACS Nano **10**, 6897–6904 (2016).
[58]S. Gharibzadeh, B. Abdollahi Nejand, M. Jakoby, T. Abzieher, D. Hauschild, S. Moghadamzadeh, J. A. Schwenzer, P. Brenner, R. Schmager, A. A. Haghighirad *et al.*, "Record open-circuit voltage wide-bandgap perovskite solar cells utilizing 2D/3D perovskite heterostructure," Adv. Energy Mater. **9**, 1803699 (2019).
[59]F. Sahli, J. Werner, B. A. Kamino, M. Bräuninger, R. Monnard, B. Paviet-Salomon, L. Barraud, L. Ding, J. J. D. Leon, D. Sacchetto *et al.*, "Fully textured monolithic perovskite/silicon tandem solar cells with 25.2% power conversion efficiency," Nat. Mater. **17**, 820–826 (2018).
[60]A. Dutta, R. K. Behera, P. Pal, S. Baitalik, and N. Pradhan, "Near-unity photoluminescence quantum efficiency for all $CsPbX_3$ (X = Cl, Br, and I) perovskite nanocrystals: A generic synthesis approach," Angew. Chem. **131**, 5608–5612 (2019).
[61]H. Wei, Y. Fang, P. Mulligan, W. Chuirazzi, H. H. Fang, C. Wang, B. R. Ecker, Y. Gao, M. A. Loi, L. Cao, and J. Huang, "Sensitive X-ray detectors made of methylammonium lead tribromide perovskite single crystals," Nat. Photonics **10**, 333–339 (2016).
[62]J. Lu, X. Sheng, G. Tong, Z. Yu, X. Sun, L. Yu, X. Xu, J. Wang, J. Xu, Y. Shi, and K. Chen, "Ultrafast solar-blind ultraviolet detection by inorganic perovskite $CsPbX_3$ quantum dots radial junction architecture," Adv. Mater. **29**, 1700400 (2017).
[63]T. Yang, Y. Zheng, Z. Du, W. Liu, Z. Yang, F. Gao, L. Wang, K. C. Chou, X. Hou, and W. Yang, "Superior photodetectors based on all-inorganic perovskite $CsPbI_3$ nanorods with ultrafast response and high stability," ACS Nano **12**, 1611–1617 (2018).
[64]F. Cao, J. Chen, D. Yu, S. Wang, X. Xu, J. Liu, Z. Han, B. Huang, Y. Gu, K. L. Choy, and H. Zeng, "Bionic detectors based on low-bandgap inorganic perovskite for selective NIR-I photon detection and imaging," Adv. Mater. **32**, 1905362 (2020).
[65]N. Ding, W. Xu, D. Zhou, G. Pan, D. Li, Y. Ji, X. Chen, D. Yang, X. Bai, C.-G. Ma, and H. Song, "Upconversion ladder enabled super-sensitive narrowband near-infrared photodetectors based on rare earth doped florine perovskite nanocrystals," Nano Energy **76**, 105103 (2020).
[66]E. Armstrong and C. O'Dwyer, "Artificial opal photonic crystals and inverse opal structures—Fundamentals and applications from optics to energy storage," J. Mater. Chem. C **3**, 6109–6143 (2015).
[67]S. Hou, A. Xie, Z. Xie, L. Y. Tobing, J. Zhou, L. Tjahjana, J. Yu, C. Hettiarachchi, D. Zhang, C. Dang *et al.*, "Concurrent inhibition and redistribution of spontaneous emission from all inorganic perovskite photonic crystals," ACS Photonics **6**, 1331–1337 (2019).
[68]C. Zhao, Y. Ma, Y. Wang, X. Zhou, H. Li, M. Li, and Y. Song, "Research progress of photonic crystal solar cells," Acta Chim. Sin. **76**, 9–21 (2018).
[69]D. Vila-Liarte, M. W. Feil, A. Manzi, J. L. Garcia-Pomar, H. Huang, M. Döblinger, L. M. Liz-Marzán, J. Feldmann, L. Polavarapu, and A. Mihi, "Templated-assembly of $CsPbBr_3$ perovskite nanocrystals into 2D photonic supercrystals with amplified spontaneous emission," Angew. Chem., Int. Ed. **59**, 17750–17756 (2020).
[70]W. Wang and L. Qi, "Light management with patterned micro-and nanostructure arrays for photocatalysis, photovoltaics, and optoelectronic and optical devices," Adv. Funct. Mater. **29**, 1807275 (2019).
[71]W. Liu, H. Ma, and A. Walsh, "Advance in photonic crystal solar cells," Renewable Sustainable Energy Rev. **116**, 109436 (2019).
[72]E. Yablonovitch, "Inhibited spontaneous emission in solid-state physics and electronics," Phys. Rev. Lett. **58**, 2059 (1987).
[73]S. John, "Strong localization of photons in certain disordered dielectric superlattices," Phys. Rev. Lett. **58**, 2486 (1987).
[74]A. Blanco, E. Chomski, S. Grabtchak, M. Ibisate, S. John, S. W. Leonard, C. Lopez, F. Meseguer, H. Miguez, J. P. Mondia *et al.*, "Large-scale synthesis of a silicon photonic crystal with a complete three-dimensional bandgap near 1.5 micrometres," Nature **405**, 437–440 (2000).
[75]P. Lodahl, A. F. Van Driel, I. S. Nikolaev, A. Irman, K. Overgaag, D. Vanmaekelbergh, and W. L. Vos, "Controlling the dynamics of spontaneous emission from quantum dots by photonic crystals," Nature **430**, 654–657 (2004).
[76]J. Liu, M. Yao, and L. Shen, "Third generation photovoltaic cells based on photonic crystals," J. Mater. Chem. C **7**, 3121–3145 (2019).
[77]D. Li, D. Zhou, W. Xu, X. Chen, G. Pan, X. Zhou, N. Ding, and H. Song, "Plasmonic photonic crystals induced two-order fluorescence enhancement of blue perovskite nanocrystals and its application for high-performance flexible ultraviolet photodetectors," Adv. Funct. Mater. **28**, 1804429 (2018).
[78]C. Cho, B. Zhao, G. D. Tainter, J.-Y. Lee, R. H. Friend, D. Di, F. Deschler, and N. C. Greenham, "The role of photon recycling in perovskite light-emitting diodes," Nat. Commun. **11**, 611 (2020).
[79]J. Tian, G. Adamo, H. Liu, M. Wu, M. Klein, J. Deng, N. S. S. Ang, R. Paniagua-Dominguez, H. Liu, A. I. Kuznetsov, and C. Soci, "Phase-change perovskite microlaser with tunable polarization vortex," Adv. Mater. e2207430 (2022).

[80]G. Long, G. Adamo, J. Tian, M. Klein, H. N. S. Krishnamoorthy, E. Feltri, H. Wang, and C. Soci, "Perovskite metasurfaces with large superstructural chirality," Nat. Commun. **13**, 1551 (2022).

[81]G. Long, R. Sabatini, M. I. Saidaminov, G. Lakhwani, A. Rasmita, X. Liu, E. H. Sargent, and W. Gao, "Chiral-perovskite optoelectronics," Nat. Rev. Mater. **5**(6), 423–439 (2020).

[82]S. D. Stranks, S. M. Wood, K. Wojciechowski, F. Deschler, M. Saliba, H. Khandelwal, J. B. Patel, S. J. Elston, L. M. Herz, M. B. Johnston *et al.*, "Enhanced amplified spontaneous emission in perovskites using a flexible cholesteric liquid crystal reflector," Nano Lett. **15**, 4935–4941 (2015).

[83]M. S. Alias, Y. Yang, T. K. Ng, I. Dursun, D. Shi, M. I. Saidaminov, D. Priante, O. M. Bakr, and B. S. Ooi, "Enhanced etching, surface damage recovery, and submicron patterning of hybrid perovskites using a chemically gas-assisted focused-ion beam for subwavelength grating photonic applications," J. Phys. Chem. Lett. **7**, 137–142 (2016).

[84]X. Chen, S. Yang, Y. C. Zheng, Y. Chen, Y. Hou, X. H. Yang, and H. G. Yang, "Multifunctional inverse opal-like TiO_2 electron transport layer for efficient hybrid perovskite solar cells," Adv. Sci. **2**, 1500105 (2015).

[85]W. Zhang, M. Anaya, G. Lozano, M. E. Calvo, M. B. Johnston, H. Míguez, and H. J. Snaith, "Highly efficient perovskite solar cells with tunable structural color," Nano Lett. **15**, 1698–1702 (2015).

[86]H. Wang, R. Haroldson, B. Balachandran, A. Zakhidov, S. Sohal, J. Y. Chan, A. Zakhidov, and W. Hu, "Nanoimprinted perovskite nanograting photodetector with improved efficiency," ACS Nano **10**, 10921–10928 (2016).

[87]S. Chen, K. Roh, J. Lee, W. K. Chong, Y. Lu, N. Mathews, T. C. Sum, and A. Nurmikko, "A photonic crystal laser from solution based organo-lead iodide perovskite thin films," ACS Nano **10**, 3959–3967 (2016).

[88]K. Chen, S. Schünemann, and H. Tüysüz, "Preparation of waterproof organometal halide perovskite photonic crystal beads," Angew. Chem., Int. Ed. **56**, 6648–6652 (2017).

[89]S. Zhou, R. Tang, and L. Yin, "Slow-photon-effect-induced photoelectrical-conversion efficiency enhancement for carbon-quantum-dot-sensitized inorganic $CsPbBr_3$ inverse opal perovskite solar cells," Adv. Mater. **29**, 1703682 (2017).

[90]L. Zheng and Y. Xuan, "Suppressing the negative effect of UV light on perovskite solar cells via photon management," Sol. Energy **173**, 1216–1224 (2018).

[91]D. H. Chun, Y. J. Choi, Y. In, J. K. Nam, Y. J. Choi, S. Yun, W. Kim, D. Choi, D. Kim, H. Shin *et al.*, "Halide perovskite nanopillar photodetector," ACS Nano **12**, 8564–8571 (2018).

[92]D. H. Choi, S. K. Nam, K. Jung, and J. H. Moon, "2D photonic crystal nanodisk array as electron transport layer for highly efficient perovskite solar cells," Nano Energy **56**, 365–372 (2019).

[93]S. Nanz, R. Schmager, M. G. Abebe, C. Willig, A. Wickberg, A. Abass, G. Gomard, M. Wegener, U. W. Paetzold, and C. Rockstuhl, "Photon recycling in nanopatterned perovskite thin-films for photovoltaic applications," APL Photonics **4**, 076104 (2019).

[94]Q. Zhang, M. M. Tavakoli, L. Gu, D. Zhang, L. Tang, Y. Gao, J. Guo, Y. Lin, S.-F. Leung, S. Poddar *et al.*, "Efficient metal halide perovskite light-emitting diodes with significantly improved light extraction on nanophotonic substrates," Nat. Commun. **10**, 727 (2019).

[95]Z. Liu, L. Wu, X. Wang, Q. Xu, Y. Hu, K. Meng, and G. Chen, "Improving efficiency and stability of colorful perovskite solar cells with two-dimensional photonic crystals," Nanoscale **12**, 8425–8431 (2020).

[96]H. Oh, H. J. Kim, S. Kim, J. A. Kim, G. Kang, and M. Park, "Highly flexible and stable perovskite/microbead hybrid photodetectors with improved interfacial light trapping," Appl. Surf. Sci. **544**, 148850 (2021).

[97]Z. Wang, Z. Wei, Y. Cai, L. Wang, M. Li, P. Liu, R. Xie, L. Wang, G. Wei, and H. Y. Fu, "Encapsulation-enabled perovskite–PMMA films combining a micro-led for high-speed white-light communication," ACS Appl. Mater. Interfaces **13**(45), 54143–54151 (2021).

[98]N. Daem, A. Mayer, G. Spronck, P. Colson, J. Loicq, C. Henrist, R. Cloots, A. Maho, M. Lobet, and J. Dewalque, "Inverse opal photonic nanostructures for enhanced light harvesting in $CH_3NH_3PbI_3$ perovskite solar cells," ACS Appl. Nano Mater. **5**(9), 13583–13593 (2022).

[99]L. Rayleigh, "XXVI. On the remarkable phenomenon of crystalline reflexion described by Prof. Stokes," London, Edinburgh, Dublin Philos. Mag. J. Sci. **26**, 256–265 (1888).

[100]L. Torrijos-Morán, A. Griol, and J. García-Rupérez, "Slow light bimodal interferometry in one-dimensional photonic crystal waveguides," Light **10**, 16 (2021).

[101]J. Joannopoulos, S. Johnson, J. Winn, and R. Meade, *Photonic Crystals: Molding Flow of Light*, 2nd ed. (Princeton University Press 2007), pp. 1–302.

[102]M. Kim, Z. Jacob, and J. Rho, "Recent advances in 2D, 3D and higher-order topological photonics," Light **9**, 130 (2020).

[103]E. Yablonovitch, T. Gmitter, and K. M. Leung, "Photonic band structure: The face-centered-cubic case employing nonspherical atoms," Phys. Rev. Lett. **67**, 2295 (1991).

[104]T. F. Krauss, M. Richard, and S. Brand, "Two-dimensional photonic-bandgap structures operating at near-infrared wavelengths," Nature **383**, 699–702 (1996).

[105]F. Amrani, J. H. Osorio, F. Delahaye, F. Giovanardi, L. Vincetti, B. Debord, F. Gerome, and F. Benabid, "Low-loss single-mode hybrid-lattice hollow-core photonic-crystal fibre," Light **10**, 7 (2021).

[106]V. Astratov, V. Bogomolov, A. Kaplyanskii, A. Prokofiev, L. Samoilovich, S. Samoilovich, and Y. A. Vlasov, "Optical spectroscopy of opal matrices with CdS embedded in its pores: Quantum confinement and photonic band gap effects," Il Nuovo Cimento D **17**, 1349–1354 (1995).

[107]P. Zhou, D. Zhou, L. Tao, Y. Zhu, W. Xu, S. Xu, S. Cui, L. Xu, and H. Song, "320-fold luminescence enhancement of $[Ru(dpp)_3]Cl_2$ dispersed on PMMA opal photonic crystals and highly improved oxygen sensing performance," Light **3**, e209 (2014).

[108]A. R. Parker and H. E. Townley, "Biomimetics of photonic nanostructures," Nat. Nanotechnol. **2**, 347–353 (2007).

[109]M. Megens, J. E. Wijnhoven, A. Lagendijk, and W. L. Vos, "Fluorescence lifetimes and linewidths of dye in photonic crystals," Phys. Rev. A **59**, 4727 (1999).

[110]K. Aoki, D. Guimard, M. Nishioka, M. Nomura, S. Iwamoto, and Y. Arakawa, "Coupling of quantum-dot light emission with a three-dimensional photonic-crystal nanocavity," Nat. Photonics **2**, 688–692 (2008).

[111]X. Gan, Y. Gao, K. Fai Mak, X. Yao, R. J. Shiue, A. Van Der Zande, M. E. Trusheim, F. Hatami, T. F. Heinz, J. Hone, and D. Englund, "Controlling the spontaneous emission rate of monolayer MoS_2 in a photonic crystal nanocavity," Appl. Phys. Lett. **103**, 181119 (2013).

[112]Z. Yin, H. Li, W. Xu, S. Cui, D. Zhou, X. Chen, Y. Zhu, G. Qin, and H. Song, "Local field modulation induced three-order upconversion enhancement: Combining surface plasmon effect and photonic crystal effect," Adv. Mater. **28**, 2518–2525 (2016).

[113]P. Lova, D. Cortecchia, H. N. S. Krishnamoorthy, P. Giusto, C. Bastianini, A. Bruno, D. Comoretto, and C. Soci, "Engineering the emission of broadband 2D perovskites by polymer distributed Bragg reflectors," ACS Photonics **5**, 867–874 (2018).

[114]W. Xu, X. Chen, and H. Song, "Upconversion manipulation by local electromagnetic field," Nano Today **17**, 54–78 (2017).

[115]S. Wu, H. Xia, J. Xu, X. Sun, and X. Liu, "Manipulating luminescence of light emitters by photonic crystals," Adv. Mater. **30**, 1803362 (2018).

[116]A. David, H. Benisty, and C. Weisbuch, "Photonic crystal light-emitting sources," Rep. Prog. Phys. **75**, 126501 (2012).

[117]S. Park, J. Cho, D. Jeong, J. Jo, M. Nam, H. Rhee, J. S. Han, Y. J. Cho, B.-K. Ju, D.-H. Ko, and H. S. Jang, "Simultaneous enhancement of luminescence and stability of $CsPbBr_3$ perovskite nanocrystals via formation of perhydropolysilazane-derived nanopatterned film," Chem. Eng. J. **393**, 124767 (2020).

[118]K. Ishizaki and S. Noda, "Manipulation of photons at the surface of three-dimensional photonic crystals," Nature **460**, 367–370 (2009).

[119]C. T. Wang, K. Chen, P. Xu, F. Yeung, H. S. Kwok, and G. Li, "Fully chiral light emission from $CsPbX_3$ perovskite nanocrystals enabled by cholesteric superstructure stacks," Adv. Funct. Mater. **29**, 1903155 (2019).

[120]S. A. Veldhuis, P. P. Boix, N. Yantara, M. Li, T. C. Sum, N. Mathews, and S. G. Mhaisalkar, "Perovskite materials for light-emitting diodes and lasers," Adv. Mater. **28**(32), 6804–6834 (2016).

[121]S. Chu, W. Chen, Z. Fang, X. Xiao, Y. Liu, J. Chen, J. Huang, and Z. Xiao, "Large-area and efficient perovskite light-emitting diodes via low-temperature blade-coating," Nat. Commun. **12**, 147 (2021).

[122]Z. L. Tseng, L. C. Chen, L. W. Chao, M. J. Tsai, D. Luo, N. R. Al Amin, S. W. Liu, and K. T. Wong, "Aggregation control, surface passivation, and optimization of device structure toward near-infrared perovskite quantum-dot light-emitting diodes with an EQE up to 15.4%," Adv. Mater. **34**(18), 2109785 (2022).
[123]G. Xing, N. Mathews, S. S. Lim, N. Yantara, X. Liu, D. Sabba, M. Grätzel, S. Mhaisalkar, and T. C. Sum, "Low-temperature solution-processed wavelength-tunable perovskites for lasing," Nat. Mater. **13**(5), 476–480 (2014).
[124]N. Li, Y. Jia, Y. Guo, and N. Zhao, "Ion migration in perovskite light-emitting diodes: mechanism, characterizations, and material and device engineering," Adv. Mater. **34**(19), 2108102 (2022).
[125]W. Xu, Q. Hu, S. Bai, C. Bao, Y. Miao, Z. Yuan, T. Borzda, A. J. Barker, E. Tyukalova, Z. Hu *et al.*, "Rational molecular passivation for high-performance perovskite light-emitting diodes," Nat. Photonics **13**, 418–424 (2019).
[126]Y. Shen, L. P. Cheng, Y. Q. Li, W. Li, J. D. Chen, S. T. Lee, and J. X. Tang, "High-efficiency perovskite light-emitting diodes with synergetic outcoupling enhancement," Adv. Mater. **31**, 1901517 (2019).
[127]J. M. Richter, M. Abdi-Jalebi, A. Sadhanala, M. Tabachnyk, J. P. Rivett, L. M. Pazos-Outón, K. C. Gödel, M. Price, F. Deschler, and R. H. Friend, "Enhancing photoluminescence yields in lead halide perovskites by photon recycling and light out-coupling," Nat. Commun. **7**, 13941 (2016).
[128]Y. Wu, B. Huang, Z. Meng, S. Zhang, and S. Wu, "Inverse opal photonic crystal stabilized $CsPbX_3$ perovskite quantum dots and their application in white LED," Chem. Eng. J. **432**, 134409 (2022).
[129]Y. Liu, W. Yang, S. Xiao, N. Zhang, Y. Fan, G. Qu, and Q. Song, "Surface-emitting perovskite random lasers for speckle-free imaging," ACS Nano **13**, 10653–10661 (2019).
[130]Q. Zhang, S. T. Ha, X. Liu, T. C. Sum, and Q. Xiong, "Room-temperature near-infrared high-Q perovskite whispering-gallery planar nanolasers," Nano Lett. **14**, 5995–6001 (2014).
[131]S. Chen, C. Zhang, J. Lee, J. Han, and A. Nurmikko, "Hybrid perovskite vertical-cavity surface-emitting laser deploying nanoporous GaN dielectric reflector technology," in Conference on Lasers and Electro-Optics (CLEO): Science and Innovations, Optical Society of America, 2016.
[132]S. Chen and A. Nurmikko, "Stable green perovskite vertical-cavity surface-emitting lasers on rigid and flexible substrates," ACS Photonics **4**, 2486–2494 (2017).
[133]Z. Li, J. Moon, A. Gharajeh, R. Haroldson, R. Hawkins, W. Hu, A. Zakhidov, and Q. Gu, "Room-temperature continuous-wave operation of organometal halide perovskite lasers," ACS Nano **12**, 10968–10976 (2018).
[134]C. Becker, S. Burger, C. Barth, P. Manley, K. Jäger, D. Eisenhauer, G. Köppel, P. Chabera, J. Chen, K. Zheng, and T. Pullerits, "Nanophotonic-enhanced two-photon-excited photoluminescence of perovskite quantum dots," ACS Photonics **5**, 4668–4676 (2018).
[135]N. Pourdavoud, S. Wang, A. Mayer, T. Hu, Y. Chen, A. Marianovich, W. Kowalsky, R. Heiderhoff, H. C. Scheer, and T. Riedl, "Photonic nanostructures patterned by thermal nanoimprint directly into organo-metal halide perovskites," Adv. Mater. **29**, 1605003 (2017).
[136]X. Zhou, M. Li, K. Wang, H. Li, Y. Li, C. Li, Y. Yan, Y. Zhao, and Y. Song, "Strong photonic-band-gap effect on the spontaneous emission in 3D lead halide perovskite photonic crystals," ChemPhysChem **19**, 2101–2106 (2018).
[137]A. Mikosch, S. Ciftci, G. Tainter, R. Shivanna, B. Haehnle, F. Deschler, and A. J. C. Kuehne, "Laser emission from self-assembled colloidal crystals of conjugated polymer particles in a metal-halide perovskite matrix," Chem. Mater. **31**, 2590–2596 (2019).
[138]S. Schünemann, S. Brittman, K. Chen, E. C. Garnett, and H. Tüysüz, "Halide perovskite 3D photonic crystals for distributed feedback lasers," ACS Photonics **4**, 2522–2528 (2017).
[139]K. Robbie, D. Broer, and M. Brett, "Chiral nematic order in liquid crystals imposed by an engineered inorganic nanostructure," Nature **399**, 764–766 (1999).
[140]L. J. Chen, J. H. Dai, J. D. Lin, T. S. Mo, H. P. Lin, H. C. Yeh, Y. C. Chuang, S. A. Jiang, and C. R. Lee, "Wavelength-tunable and highly stable perovskite-quantum-dot-doped lasers with liquid crystal lasing cavities," ACS Appl. Mater. Interfaces **10**, 33307–33315 (2018).
[141]G. Grancini, C. Roldán-Carmona, I. Zimmermann, E. Mosconi, X. Lee, D. Martineau, S. Narbey, F. Oswald, F. De Angelis, M. Graetzel, and M. K. Nazeeruddin, "One-year stable perovskite solar cells by 2D/3D interface engineering," Nat. Commun. **8**, 15684 (2017).
[142]L. Wang, H. Zhou, J. Hu, B. Huang, M. Sun, B. Dong, G. Zheng, Y. Huang, Y. Chen, L. Li *et al.*, "A Eu^{3+}-Eu^{2+} ion redox shuttle imparts operational durability to Pb-I perovskite solar cells," Science **363**, 265–270 (2019).
[143]H. Tan, A. Jain, O. Voznyy, X. Lan, F. P. G. De Arquer, J. Z. Fan, R. Quintero-Bermudez, M. Yuan, B. Zhang, Y. Zhao *et al.*, "Efficient and stable solution-processed planar perovskite solar cells via contact passivation," Science **355**, 722–726 (2017).
[144]Q. Jiang, Y. Zhao, X. Zhang, X. Yang, Y. Chen, Z. Chu, Q. Ye, X. Li, Z. Yin, and J. You, "Surface passivation of perovskite film for efficient solar cells," Nat. Photonics **13**, 460–466 (2019).
[145]K. Deng, Z. Liu, M. Wang, and L. Li, "Nanoimprinted grating-embedded perovskite solar cells with improved light management," Adv. Funct. Mater. **29**, 1900830 (2019).
[146]M. Jčt, S. Albrecht, L. Kegelmann, C. M. Wolff, F. Lang, B. Lipovšek, J. Krč, L. Korte, D. Neher, B. Rech, and M. Topič, "Efficient light management by textured nanoimprinted layers for perovskite solar cells," ACS Photonics **4**, 1232–1239 (2017).
[147]P. Bermel, C. Luo, L. Zeng, L. C. Kimerling, and J. D. Joannopoulos, "Improving thin-film crystalline silicon solar cell efficiencies with photonic crystals," Opt. Express **15**(25), 16986–17000 (2007).
[148]S. Nishimura, N. Abrams, B. A. Lewis, L. I. Halaoui, T. E. Mallouk, K. D. Benkstein, J. Van de Lagemaat, and A. J. Frank, "Standing wave enhancement of red absorbance and photocurrent in dye-sensitized titanium dioxide photoelectrodes coupled to photonic crystals," J. Am. Chem. Soc. **125**(20), 6306–6310 (2003).
[149]S. Colodrero, A. Mihi, L. Häggman, M. Ocana, G. Boschloo, A. Hagfeldt, and H. Miguez, "Porous one-dimensional photonic crystals improve the power-conversion efficiency of dye-sensitized solar cells," Adv. Mater. **21**(7), 764–770 (2009).
[150]S. Colodrero, A. Forneli, C. López-López, L. Pellejà, H. Míguez, and E. Palomares, "Efficient transparent thin dye solar cells based on highly porous 1D photonic crystals," Adv. Funct. Mater. **22**(6), 1303–1310 (2012).
[151]A. Chutinan, N. P. Kherani, and S. Zukotynski, "High-efficiency photonic crystal solar cell architecture," Opt. Express **17**(11), 8871–8878 (2009).
[152]B. K. Singh, A. Bijalwan, and V. Rastogi, "Enhancement of light harvesting efficiency of perovskite solar cells by using one-dimensional photonic crystals," Appl. Opt. **58**, 8046–8054 (2019).
[153]S. Sun, Z. Xie, G. Qin, and L. Xiao, "Light trapping nano structures with over 30% enhancement in perovskite solar cells," Org. Electron. **75**, 105385 (2019).
[154]D. I. Kim, J. W. Lee, R. H. Jeong, J. H. Yu, J. W. Yang, S. H. Nam, and J. H. Boo, "Enhancing the optical properties using hemisphere TiO_2 photonic crystal as the electron acceptor for perovskite solar cell," Appl. Surf. Sci. **487**, 409–415 (2019).
[155]Y. Wang, P. Wang, X. Zhou, C. Li, H. Li, X. Hu, F. Li, X. Liu, M. Li, and Y. Song, "Solar cells: Diffraction-grated perovskite induced highly efficient solar cells through nanophotonic light trapping," Adv. Energy Mater. **8**, 1870052 (2018).
[156]N. Cefarin, A. Cian, A. Sonato, E. Sovernigo, F. Suran, Z. Teklu, A. Zanut, A. Pozzato, and M. Tormen, "Nanostructuring methylammonium lead iodide perovskite by ultrafast nano imprinting lithography," Microelectron. Eng. **176**, 106–110 (2017).
[157]M. T. Hörantner, W. Zhang, M. Saliba, K. Wojciechowski, and H. J. Snaith, "Templated microstructural growth of perovskite thin films via colloidal monolayer lithography," Energy Environ. Sci. **8**, 2041–2047 (2015).
[158]C. S. O. Ramírez Quiroz, C. Bronnbauer, I. Levchuk, Y. Hou, C. J. Brabec, and K. Forberich, "Coloring semitransparent perovskite solar cells via dielectric mirrors," ACS Nano **10**, 5104–5112 (2016).
[159]G. Y. Yoo, R. Azmi, C. Kim, W. Kim, B. K. Min, S. Y. Jang, and Y. R. Do, "Stable and colorful perovskite solar cells using a nonperiodic SiO_2/TiO_2 multi-nanolayer filter," ACS Nano **13**, 10129–10139 (2019).
[160]K. Meng, S. Gao, L. Wu, G. Wang, X. Liu, G. Chen, Z. Liu, and G. Chen, "Two-dimensional organic–inorganic hybrid perovskite photonic films," Nano Lett. **16**, 4166–4173 (2016).
[161]W. Wang, Y. He, and L. Qi, "High-efficiency colorful perovskite solar cells using TiO_2 nanobowl arrays as a structured electron transport layer," Sci. China Mater. **63**, 35–46 (2020).

[162]T. Kirchartz, F. Staub, and U. Rau, "Impact of photon recycling on the open-circuit voltage of metal halide perovskite solar cells," ACS Energy Lett. **1**, 731–739 (2016).
[163]S. Zhou, R. Tang, H. Li, L. Fu, B. Li, and L. Yin, "Fluorescence resonance energy transfer effect enhanced high performance of Si quantum dots/$CsPbBr_3$ inverse opal heterostructure perovskite solar cells," J. Power Sources **439**, 227065 (2019).
[164]M. Wang, W. Wang, B. Ma, W. Shen, L. Liu, K. Cao, S. Chen, and W. Huang, "Lead-free perovskite materials for solar cells," Nano-Micro Lett. **13**, 62 (2021).
[165]J. Zhang, X. Gao, Y. Deng, Y. Zha, and C. Yuan, "Comparison of life cycle environmental impacts of different perovskite solar cell systems," Sol. Energy Mater. Sol. Cells **166**, 9–17 (2017).
[166]A. Babayigit, D. Duy Thanh, A. Ethirajan, J. Manca, M. Muller, H. G. Boyen, and B. Conings, "Assessing the toxicity of Pb- and Sn-based perovskite solar cells in model organism *Danio rerio*," Sci. Rep. **6**(1), 18721 (2016).
[167]B. Saparov and D. B. Mitzi, "Organic–inorganic perovskites: Structural versatility for functional materials design," Chem. Rev. **116**(7), 4558–4596 (2016).
[168]D. Cortecchia, H. A. Dewi, J. Yin, A. Bruno, S. Chen, T. Baikie, P. P. Boix, M. Gratzel, S. Mhaisalkar, C. Soci, and N. Mathews, "Lead-free $MA_2CuCl_{(x)}Br_{(4-x)}$ hybrid perovskites," Inorg. Chem. **55**(3), 1044–1052 (2016).
[169]C. Li, Y. Ma, Y. Xiao, L. Shen, and L. Ding, "Advances in perovskite photodetectors," InfoMat **2**, 1247–1256 (2020).
[170]X. Hu, X. Zhang, L. Liang, J. Bao, S. Li, W. Yang, and Y. Xie, "High-performance flexible broadband photodetector based on organolead halide perovskite," Adv. Funct. Mater. **24**, 7373–7380 (2014).
[171]R. Liu, H. Zhou, Z. Song, X. Yang, D. Wu, Z. Song, H. Wang, and Y. Yan, "Low-reflection (110)-orientation-preferred $CsPbBr_3$ nanonet films for application in high-performance perovskite photodetectors," Nanoscale **11**, 9302–9309 (2019).
[172]Y. Zhan, Y. Wang, Q. Cheng, C. Li, K. Li, H. Li, J. Peng, B. Lu, Y. Wang, Y. Song, L. Jiang, and M. Li, "A butterfly-inspired hierarchical light-trapping structure towards a high-performance polarization-sensitive perovskite photodetector," Angew. Chem. **131**, 16608–16614 (2019).
[173]J. Zeng, C. Meng, X. Li, Y. Wu, S. Liu, H. Zhou, H. Wang, and H. Zeng, "Interfacial-tunneling-effect-enhanced $CsPbBr_3$ photodetectors featuring high detectivity and stability," Adv. Funct. Mater. **29**, 1904461 (2019).
[174]J. Zeng, X. Li, Y. Wu, D. Yang, Z. Sun, Z. Song, H. Wang, and H. Zeng, "Space-confined growth of $CsPbBr_3$ film achieving photodetectors with high performance in all figures of merit," Adv. Funct. Mater. **28**, 1804394 (2018).
[175]Y. Ji, D. Zhou, N. Wang, N. Ding, W. Xu, and H. Song, "Flexible double narrowband near-infrared photodetector based on PMMA/core–shell upconversion nanoparticle composites," J. Rare Earths **40**(2), 211–217 (2022).